Dos galaxias de la Vía Láctea: FORNAX Y SCULPTOR

Física Teórica

Integrantes: Rosa Linda Merma Ccamaqque
Dr. Elmer Luque Canaza

November 8, 2022

Universidad Nacional de San Agustín de Arequipa
Facultad de Ciencias Naturales y Formales
Escuela Profesional de Física

Contenido

Introducción

Ubicación

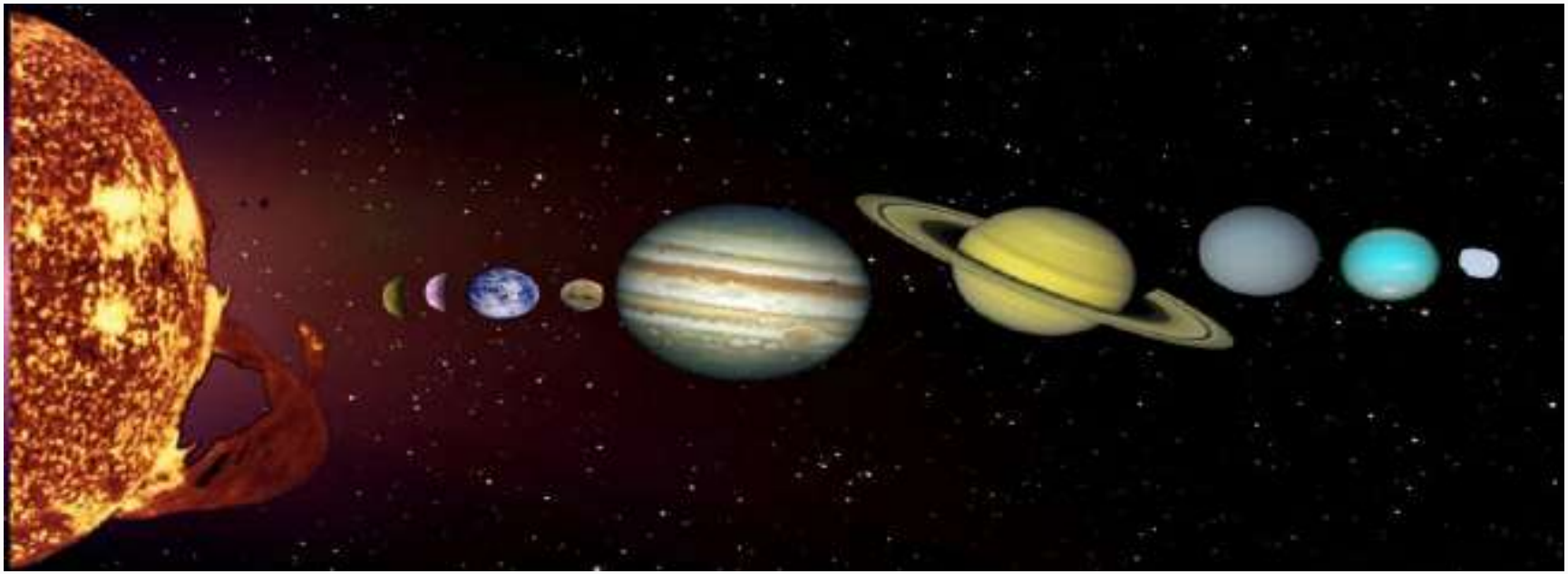

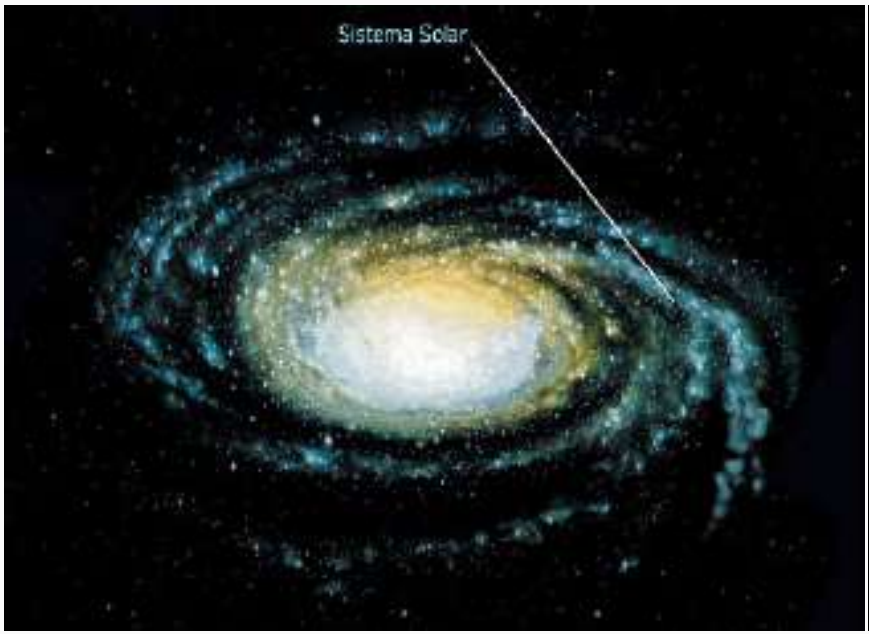
Sistema Solar

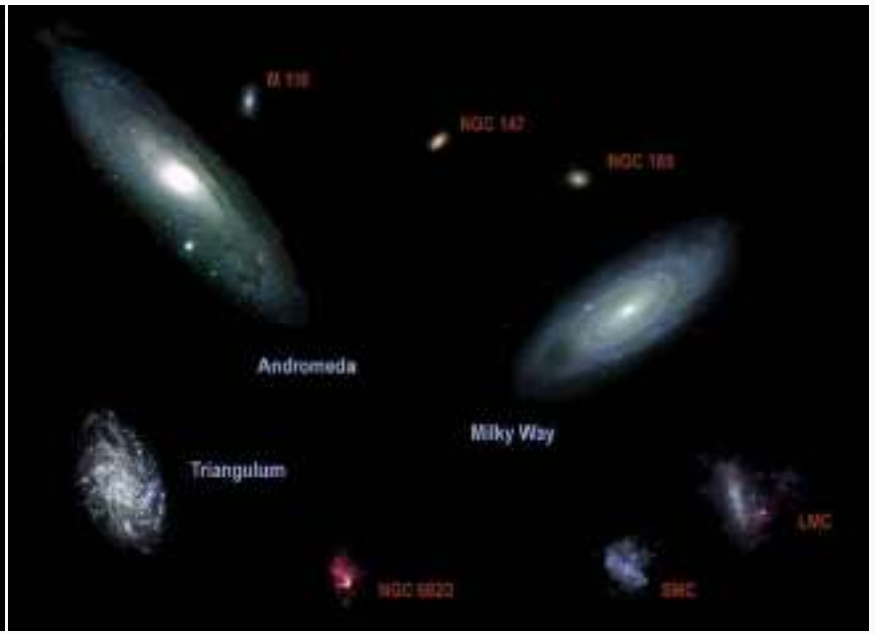
M 110
NGC 147
NGC 185
Andromeda
Milky Way
Triangulum
LMC
NGC 6822
SMC

Ubicación

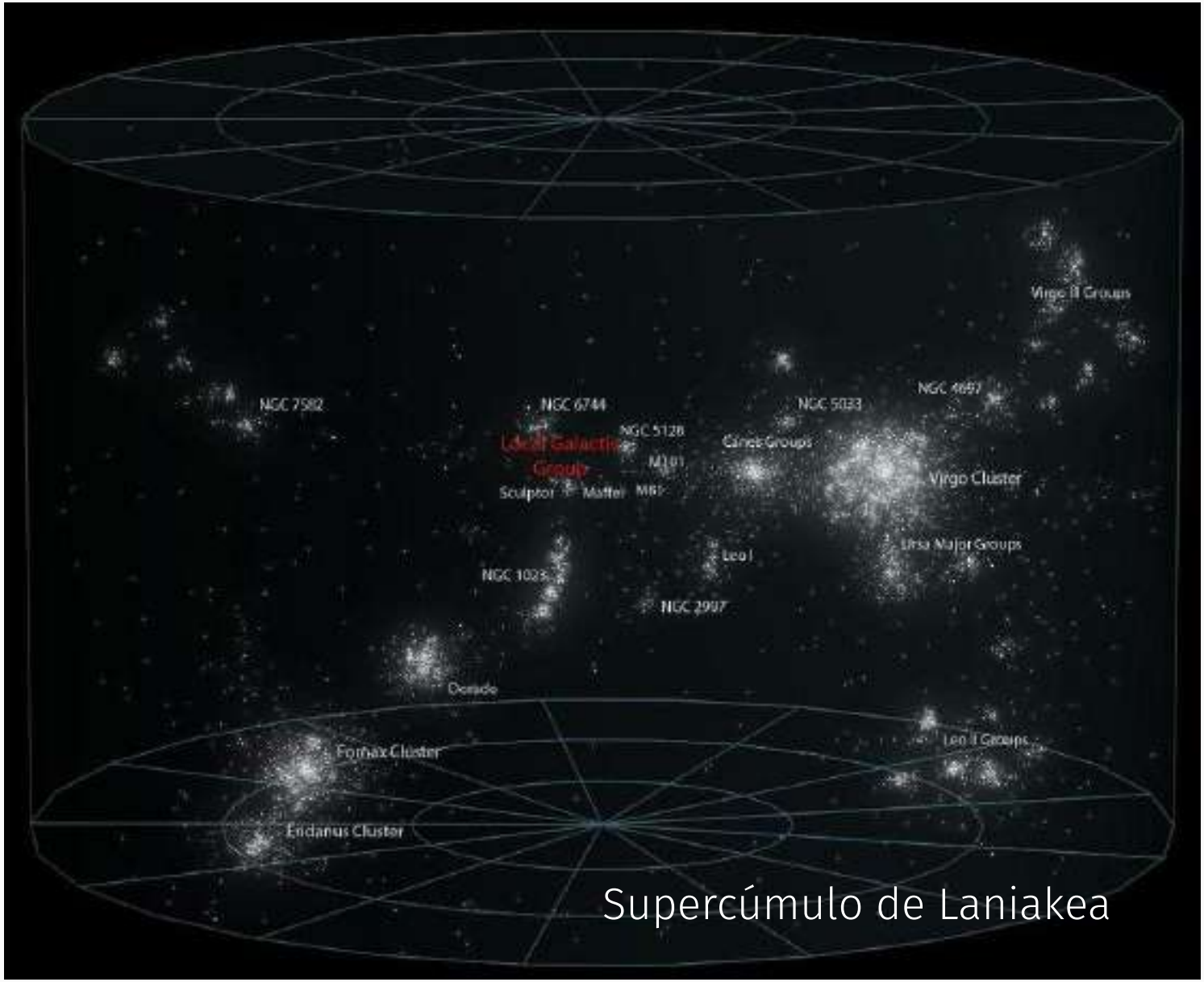

Supercúmulo de Laniakea

Galaxias

Galaxias

Figure 1: Vía Láctea[1]

[1] https://www.muyinteresante.es/ciencia/fotos/cosas-que-no-sabias-sobre-la-via-lactea

Galaxias

Figure 2: Catálogo de nebulosa y cúmulos de estrellas [2]

[2] https://e.captchasee.live/video/?c=1294a368-7485-4e8c-9e9d-73dd3860d295a=l143904

Galaxias

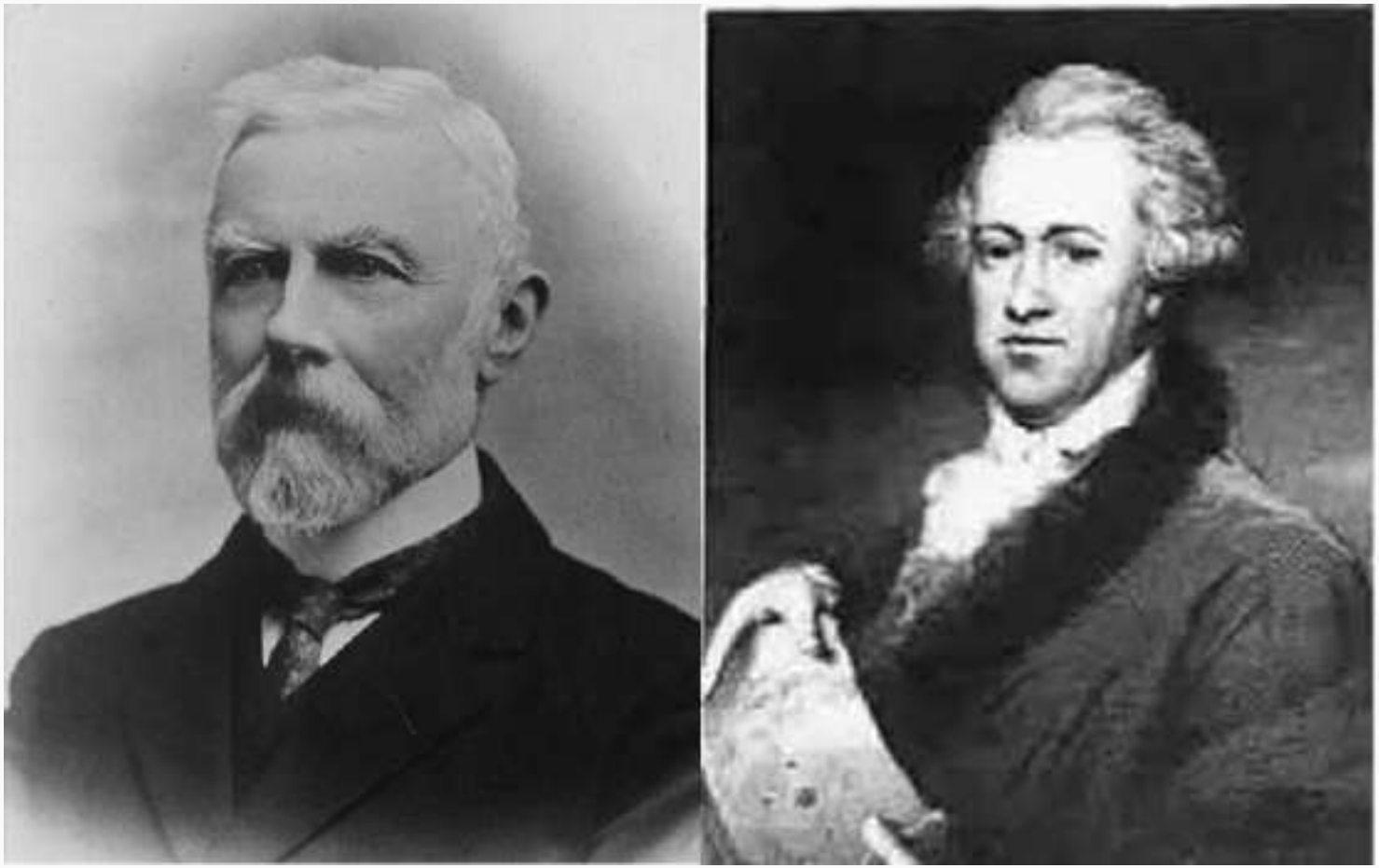

Figure 3: John Louis Emil Dreyer [3] y William Herschel[4]

[3] https://link.springer.com/referenceworkentry/10.1007/978-1-4419-9917-7_382
[4] https://www.ecured.cu/William_Herschel

Galaxias

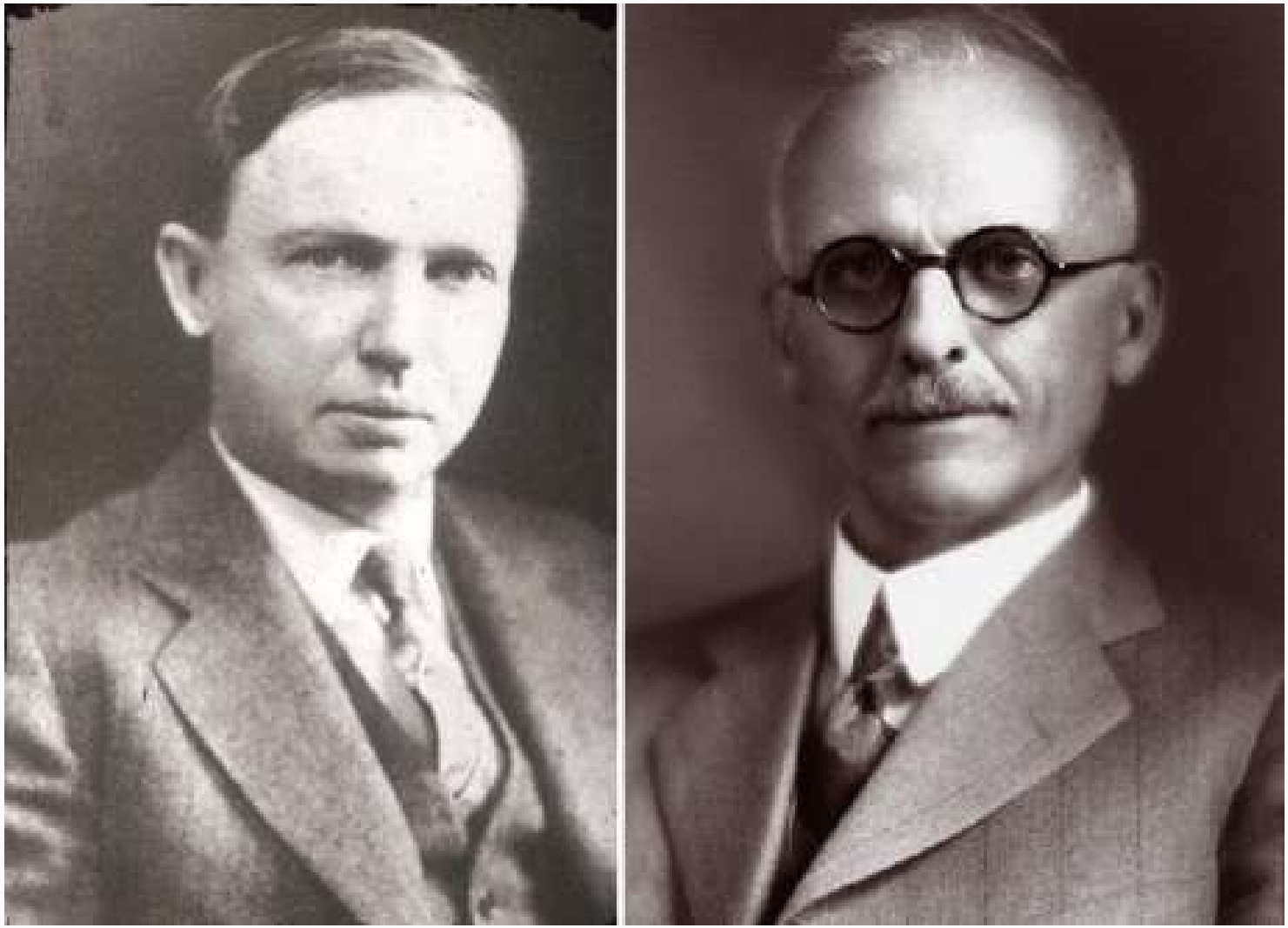

Figure 4: Harlow Shapley y Heber Curtis [5]

[5] http://laaventuradelaciencia.blogspot.com/2016/09/harlow-shapley-ii-el-gran-debate.html

Galaxias

El gran debate [6]

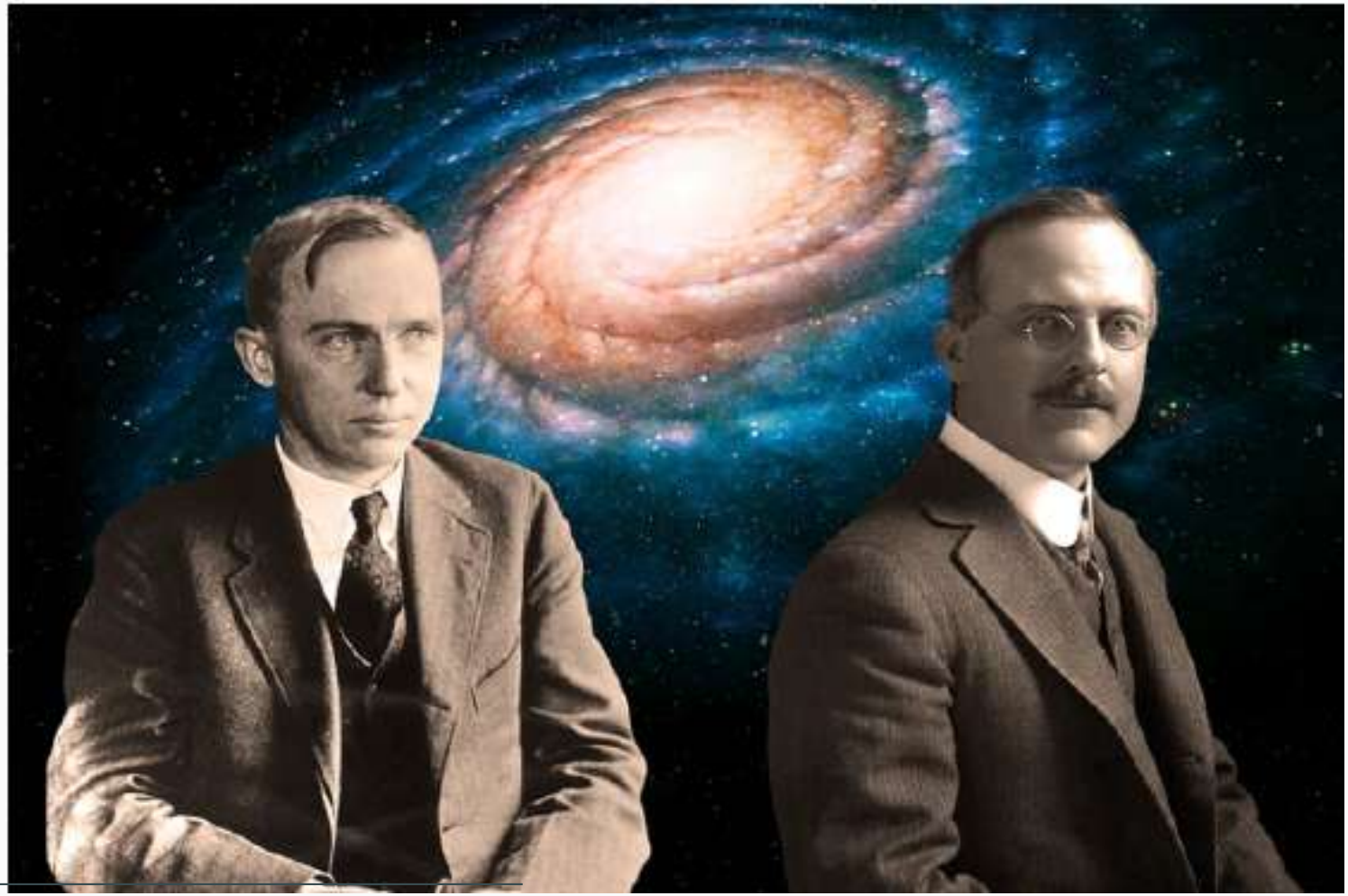

[6] https://youtu.be/cBa932gXEM0

Galaxias

(a) Edwin Hubble [7]

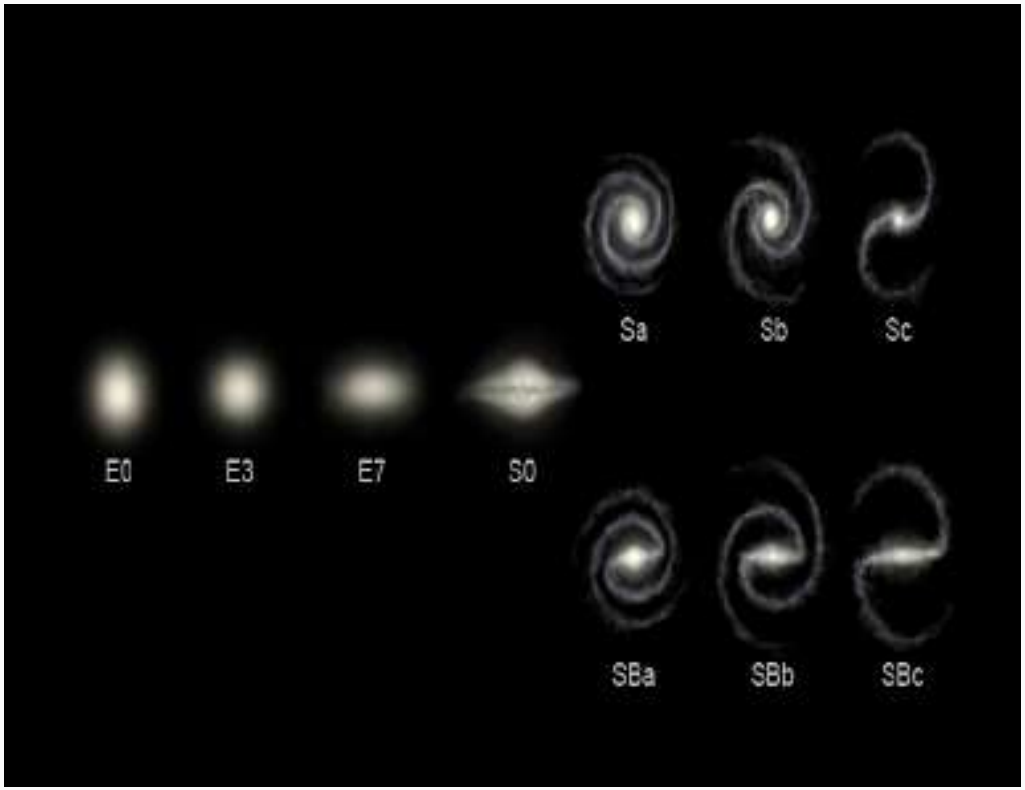

(b) Secuencia de Hubble [8]

[7] https://elpais.com/sociedad/2011/12/07/actualidad/1323277752_0 02602.*html*

[8] https://es.wikipedia.org/wiki/Secuencia_de_Hubble/media/Archivo : *Hubble_Sequence_Photo.png*

Algunos grandes proyectos de observaciones

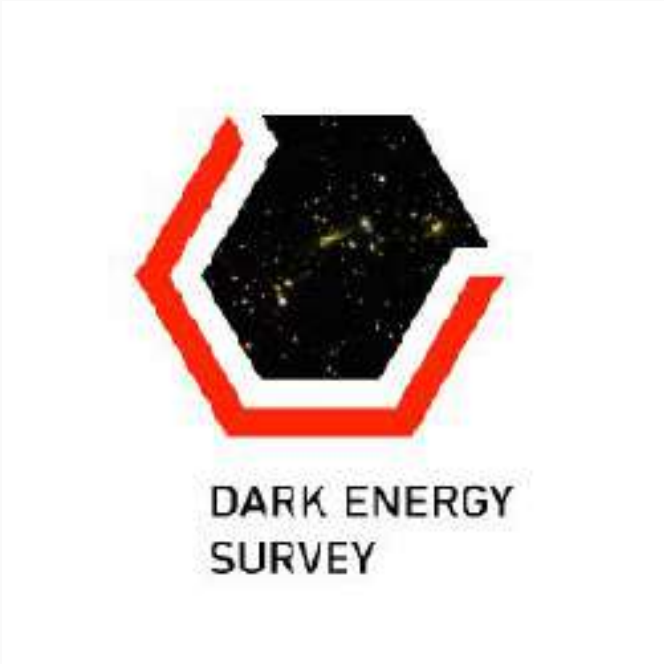

(c) Dark Energy Survey [9]

(d) Sloan Digital Sky Survey [10]

[9] https://www.darkenergysurvey.org/es/

[10] https://www.sdss.org/


¿Cuál es el origen del Universo?

Introducción a las galaxias enanas

Modelo cosmológico de la Materia Oscura Fría (CDM, Cold Dark Matter)

Introducción a las galaxias enanas

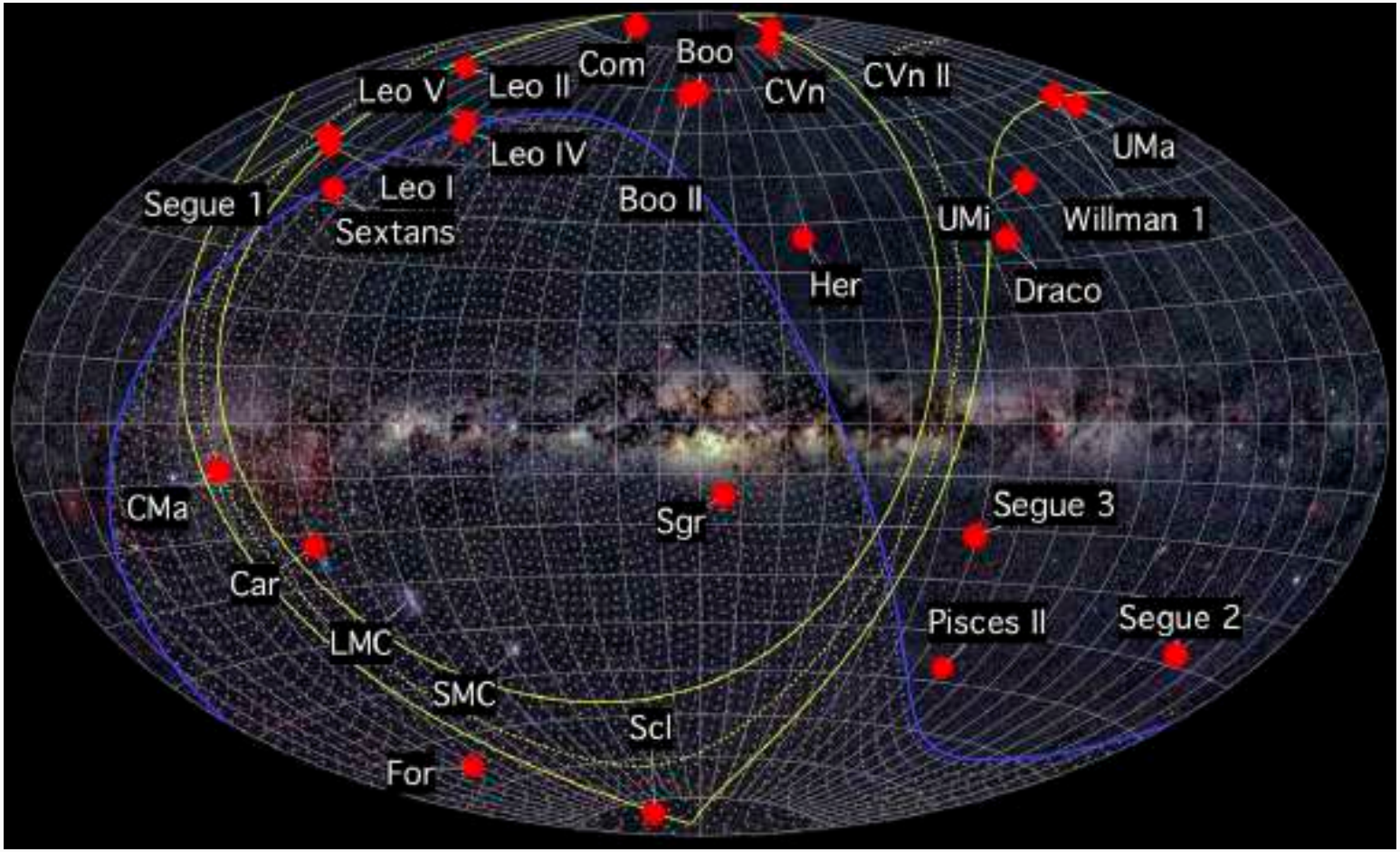

Figure 5: Distribucion espacial de las galaxias enanas conocidas en el halo de la Vía Láctea [11]

[11] https://www.investigacionyciencia.es/blogs/astronomia/17/posts/el-dark-energy-survey-encuentra-nuevas-galaxias-enanas-orbitando-la-va-lctea-13476

Galaxias enanas

Galaxias enanas

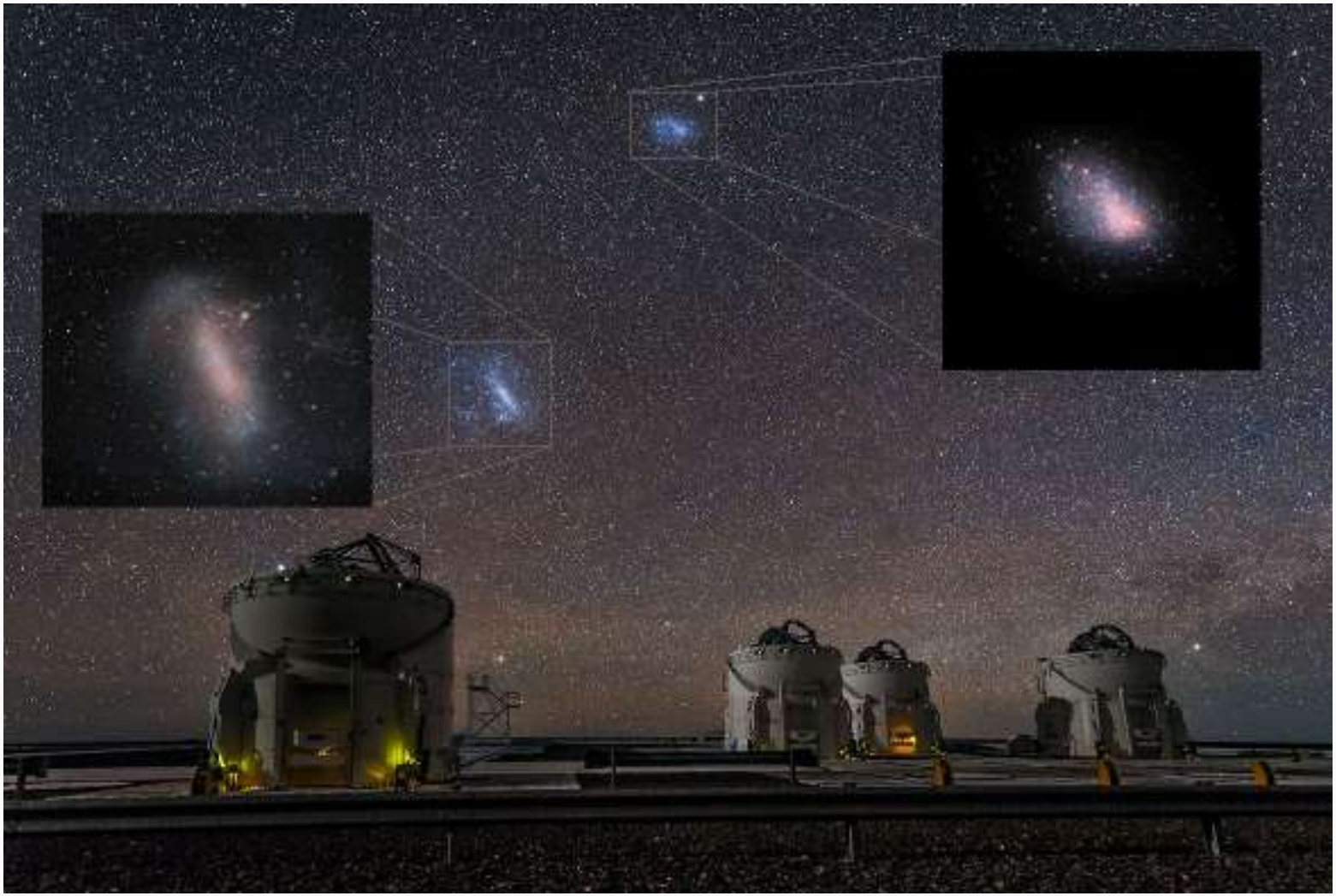

Figure 6: Pequeña y Gran nube de Magallanes [12]

[12] https://www.tercerainformacion.es/articulo/ciencia/05/01/2019/la-gran-nube-de-magallanes-se-adelantara-a-andromeda-en-su-impacto-con-la-via-lactea/

Galaxias enanas

(a) Galaxia enana esferoidal Sculptor (b) Galaxia enana esferoidal Fornax [13]

[13] https://desportal2.cosmology.illinois.edu/dri/api/api-auth/login/?next=/sky/

Fornax y Sculptor

En la literatura se realizaron estudios fotométricos y espectroscópicos para Fornax y Sculptor

¡Aquí nos ocuparemos de los estudios fotométricos!

Algunos trabajos realizados

1961AJ.....66...83H

THE ASTRONOMICAL JOURNAL VOLUME 66, NUMBER 2 MARCH, 1961

The Fornax Dwarf Galaxy. I. The Globular Clusters

PAUL W. HODGE*
Harvard College Observatory, Cambridge Massachusetts, and Mount Wilson and Palomar Observatories, Carnegie Institution of Washington, California Institute of Technology

(Received December 15, 1960)

Two new globular clusters have been found to belong to the Fornax dwarf galaxy. The properties and dimensions of the five known globular clusters are comparable to those of our galaxy. Measures of individual stars in each indicate that the magnitudes of their brightest stars are identical within 0.1 mag., but that the brightest stars of the main galaxy are 0.5 mag. brighter. The globular clusters have nearly ten times the projected star density of the main galaxy.

SHORTLY after Shapley's discovery (1938) of the nearby dwarf elliptical galaxy in Fornax, he published the positions of three globular clusters apparently associated with this galaxy (1939). Two of these clusters were investigated by Baade and Hubble (1939), who used the Mt. Wilson 100-inch reflector.

Neither the 100-inch telescope nor Harvard's 60-inch reflector, used by Shapley, has a large enough field to photograph the entire galaxy on one plate. Therefore it was thought worthwhile to re-examine the Fornax dwarf with plates of the ADH Baker-Schmidt, which has both a large field and a faint magnitude limit. Two long-exposure ADH plates, taken without filter, were examined in 1957, and then a series of very long-exposure blue and visual ADH plates was taken of the Fornax galaxy when the writer was in South Africa in 1958. In addition, he has taken a few plates of the galaxy with the 48-inch Schmidt of the Palomar Ob-

plates. Cluster No. 5 is very heavily concentrated towards its center, and appears nearly stellar on plates of the 24-inch Bruce camera.

The other new cluster, No. 1, is unusually open and poor in stars. It has a very irregular appearance, but is quite certainly a globular cluster, for its brightest stars are similar in magnitude and color to those of the other four globulars. Cluster No. 1 is 43′ distant from the center of the Fornax galaxy and lies about 5′ from the outermost portions of the galaxy traceable from star counts.

It seems unlikely that any further globular clusters will be found to be members of the Fornax dwarf. The sky within 2° of the center of the system was thoroughly searched on ADH plates with a limiting photographic magnitude of about 20, without additions to the present list.

A very faint object, just 7′ north of cluster 4, was

Algunos trabajos realizados

The Astronomical Journal, 130:1065–1082, 2005 September
© 2005. The American Astronomical Society. All rights reserved. Printed in U.S.A.

THE ABSENCE OF EXTRATIDAL STRUCTURE IN THE SCULPTOR DWARF SPHEROIDAL GALAXY

M. G. Coleman and G. S. Da Costa
Research School of Astronomy and Astrophysics, Institute of Advanced Studies, Australian National University, Cotter Road, Weston Creek, ACT 2611, Australia; coleman@mso.anu.edu.au, gdc@mso.anu.edu.au

and

Joss Bland-Hawthorn
Anglo-Australian Observatory, P.O. Box 296, Epping, NSW 2121, Australia; jbh@aaocpp.aao.gov.au
Received 2005 January 13; accepted 2005 June 2

ABSTRACT

The results of a wide-field survey of the Sculptor dwarf spheroidal galaxy are presented. Our aims were to obtain an accurate map of the outer structure of Sculptor and to determine the level of interaction between this system and the Galaxy. Photometry was obtained in two colors down to the magnitude limits of $V = 20$ and $I = 19$, covering a $3.^{\circ}1 \times 3.^{\circ}1$ area centered on Sculptor. The resulting color-magnitude data were used as a mask to select candidate horizontal-branch (HB) and red giant branch stars for this system. Previous work has shown that the red HB stars are more concentrated than the blue HB stars. We have determined the radial distributions of these two populations and show that the overall Sculptor density profile is well described by a two-component model based on a combination of these radial distributions. In addition, spectra of the Ca II triplet region were obtained for over 700 candidate red giant stars over the 10 deg^2 region using the 2dF instrument on the Anglo-Australian Telescope. These spectra were used to remove foreground Galactic stars based on radial velocity and Ca II triplet strength. The final list of Sculptor members contains 148 stars, 7 of which are located beyond the nominal tidal radius. Both the photometric and spectroscopic data sets indicate no significant extratidal structure. These results support at most a mild level of interaction between this system and the Galaxy, and we have measured an upper mass limit for extratidal material to be 2.3% ± 0.6% of the Sculptor luminous mass. This lack of tidal interaction indicates that previous velocity dispersion measurements (and hence the amount of dark matter detected) in this system are not strongly influenced by the Galactic tidal field.

Key words: galaxies: dwarf — galaxies: individual (Sculptor) — galaxies: interactions — galaxies: photometry — galaxies: stellar content — Galaxy: halo — Local Group

Online material: color figures, machine-readable table

Algunos trabajos realizados

The Astrophysical Journal, 860:66 (54pp), 2018 June 10 https://doi.org/10.3847/1538-4357/aac16b
© 2018. The American Astronomical Society. All rights reserved.

A MegaCam Survey of Outer Halo Satellites. III. Photometric and Structural Parameters*†

Ricardo R. Muñoz[1,2], Patrick Côté[3], Felipe A. Santana[1], Marla Geha[2], Joshua D. Simon[4], Grecco A. Oyarzún[1], Peter B. Stetson[3], and S. G. Djorgovski[5]

[1] Departamento de Astronomía, Universidad de Chile, Camino del Observatorio 1515, Las Condes, Santiago, Chile; rmunoz@das.uchile.cl
[2] Astronomy Department, Yale University, New Haven, CT 06520, USA
[3] National Research Council of Canada, Herzberg Astronomy & Astrophysics Program, 5071 W. Saanich Road, Victoria, BC, V9E 2E7, Canada
[4] Observatories of the Carnegie Institution of Washington, 813 Santa Barbara St., Pasadena, CA 91101, USA
[5] Astronomy Department, California Institute of Technology, Pasadena, CA 91125, USA

Received 2017 August 10; revised 2018 April 28; accepted 2018 April 30; published 2018 June 12

Abstract

We present structural parameters from a wide-field homogeneous imaging survey of Milky Way satellites carried out with the MegaCam imagers on the 3.6 m Canada–France–Hawaii Telescope and 6.5 m Magellan-Clay telescope. Our survey targets an unbiased sample of "outer halo" satellites (i.e., substructures having galactocentric distances greater than 25 kpc) and includes classical dSph galaxies, ultra-faint dwarfs, and remote globular clusters. We combine deep, panoramic *gr* imaging for 44 satellites and archival *gr* imaging for 14 additional objects (primarily obtained with the DECam instrument as part of the Dark Energy Survey) to measure photometric and structural parameters for 58 outer halo satellites. This is the largest and most uniform analysis of Milky Way satellites undertaken to date and represents roughly three-quarters ($58/81 \simeq 72\%$) of all known outer halo satellites. We use a maximum-likelihood method to fit four density laws to each object in our survey: exponential, Plummer, King, and Sérsic models. We systematically examine the isodensity contour maps and color–magnitude diagrams for each of our program objects, present a comparison with previous results, and tabulate our best-fit photometric and structural parameters, including ellipticities, position angles, effective radii, Sérsic indices, absolute magnitudes, and surface brightness measurements. We investigate the distribution of outer halo satellites in the size–magnitude diagram and show that the current sample of outer halo substructures spans a wide range in effective radius, luminosity, and surface brightness, with little evidence for a clean separation into star cluster and galaxy populations at the faintest luminosities and surface brightnesses.

Key words: galaxies: dwarf – galaxies: photometry – galaxies: structure – globular clusters: general – Local Group – surveys

Algunos trabajos realizados

The Astrophysical Journal, 881:118 (14pp), 2019 August 20 https://doi.org/10.3847/1538-4357/ab31a9
© 2019. The American Astronomical Society. All rights reserved.

The Morphology and Structure of Stellar Populations in the Fornax Dwarf Spheroidal Galaxy from Dark Energy Survey Data

M. Y. Wang[1,2], T. de Boer[3,4], A. Pieres[5,6], T. S. Li[7,8], A. Drlica-Wagner[7], S. E. Koposov[1,4], A. K. Vivas[9], A. B. Pace[2], B. Santiago[6,10], A. R. Walker[9], D. L. Tucker[7], L. Strigari[2], J. L. Marshall[2], B. Yanny[7], D. L. DePoy[2], K. Bechtol[11], A. Roodman[12,13], T. M. C. Abbott[9], F. B. Abdalla[14,15], S. Allam[7], J. Annis[7], S. Avila[16], E. Bertin[17,18], D. Brooks[14], D. L. Burke[12,13], A. Carnero Rosell[5,6], M. Carrasco Kind[19,20], C. E. Cunha[5], C. B. D'Andrea[21], L. N. da Costa[5,6], J. De Vicente[22], S. Desai[23], T. F. Eifler[24,25], J. Estrada[7], B. Flaugher[7], J. Frieman[7,8], J. García-Bellido[26], D. W. Gerdes[27,28], D. Gruen[12,13], R. A. Gruendl[19,20], G. Gutierrez[7], D. L. Hollowood[29], K. Honscheid[30,31], D. J. James[32], K. Kuehn[33], N. Kuropatkin[7], O. Lahav[14], M. A. G. Maia[5,6], R. Miquel[34,35], E. Sanchez[22], V. Scarpine[7], I. Sevilla-Noarbe[22], M. Smith[36], R. C. Smith[9], F. Sobreira[37,6], E. Suchyta[38], M. E. C. Swanson[20], and G. Tarle[28]
(DES Collaboration)

Abstract

Using deep wide-field photometry 3 yr data (Y3) from the Dark Energy Survey (DES), we present a panoramic study of the Fornax dwarf spheroidal galaxy. The data presented here—a small subset of the full survey—uniformly cover a region of 25 deg^2 centered on the galaxy to a depth of $g \sim 23.5$. We use these data to study the structural properties of Fornax, overall stellar population, and its member stars in different evolutionary phases. We also search for possible signs of tidal disturbance. Fornax is found to be significantly more spatially extended than what early studies suggested. No statistically significant distortions or signs of tidal disturbances were found down to a surface brightness limit of ~32.1 mag arcsec^{-2}. However, there are hints of shell-like features located ~20′–40′ from the center of Fornax that may be stellar debris from past merger events. We also find that intermediate-age and young main-sequence populations show different orientation at the galaxy center and have many substructures. The deep DES Y3 data allow us to characterize the age of those young stellar substructures with great accuracy, both those previously known and those newly identified as possible overdensities in this work, on the basis of their

Galaxia esferoidal enana Fornax

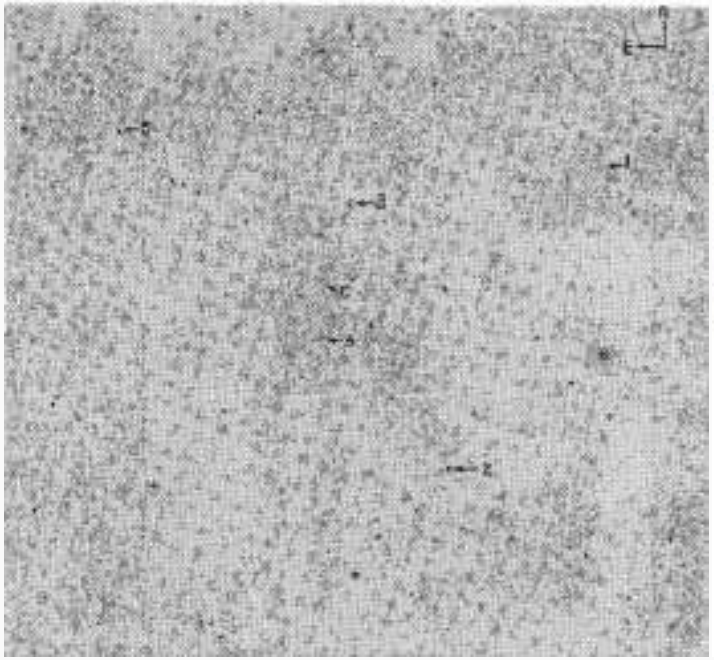

(c) Imagen fotográfica (Hodge, 1961).

(d) Imagen de CCD [14].

[14] https://desportal2.cosmology.illinois.edu/dri/api/api-auth/login/?next=/sky/

Galaxia esferoidal enana Fornax

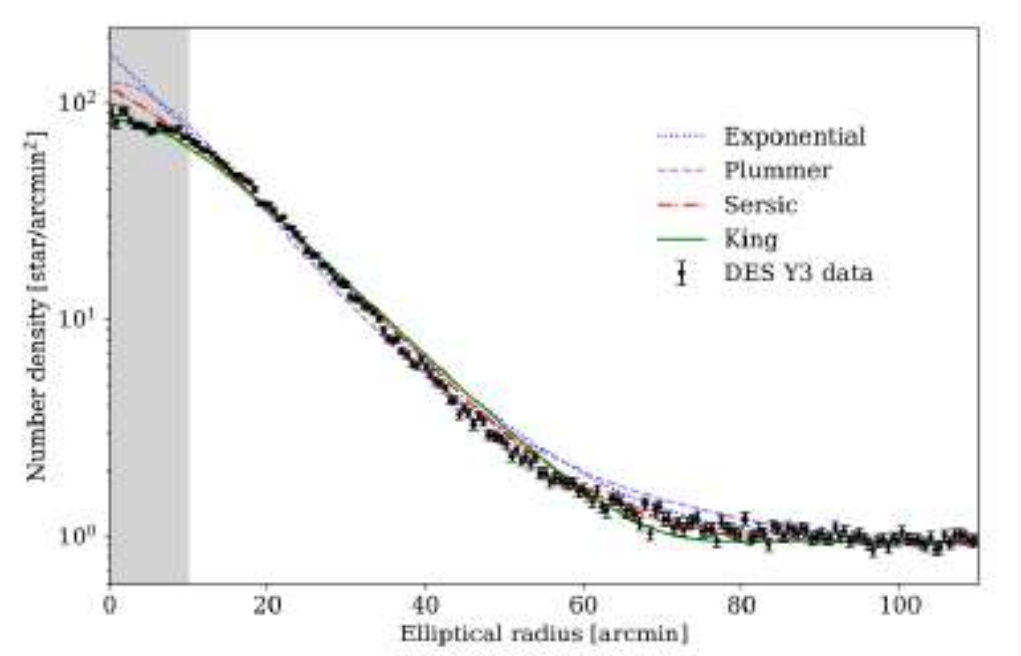

(e) Ajuste de modelos de densidad.

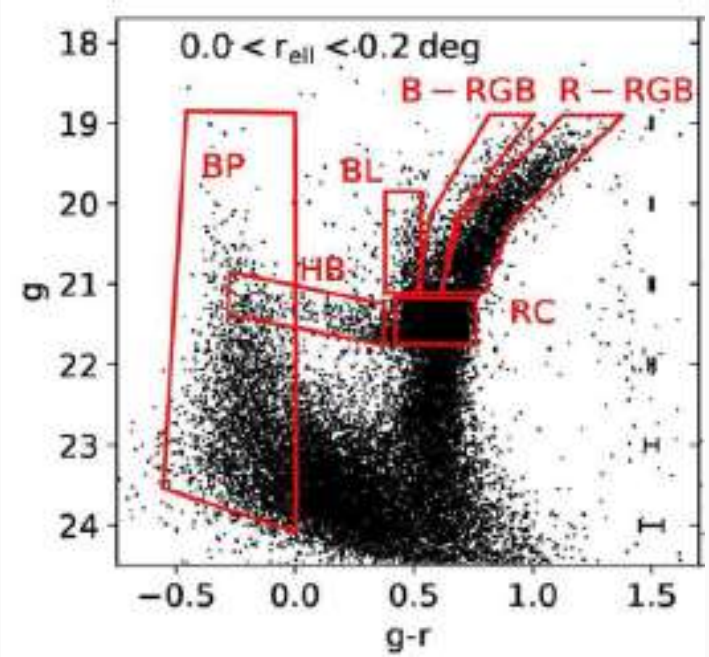

(f) Diagrama color-magnitud (Wang et al., 2019).

Datos del Dark Energy Survey (DES)

Modelos de perfil de densidad radial

$$\Sigma_{\rm exp}(r) = \Sigma_{0,e}\,\exp\left(-\frac{r}{r_e}\right), \tag{1}$$

$$\Sigma_{\rm Plummer}(r) = \Sigma_{0,P}\left(1+\frac{r^2}{r_p^2}\right)^{-2}, \tag{2}$$

$$\Sigma_{\rm King}(r) = k\left\{\frac{1}{[1+(r/r_c)^2]^{\frac{1}{2}}} - \frac{1}{[1+(r_t/r_c)^2]^{\frac{1}{2}}}\right\}^2 \tag{3}$$

$$\Sigma_{\rm Sersic}(r) = \Sigma_{0,S}\,\exp\left[-\left(\frac{r}{r_s}\right)^{1/n}\right] \tag{4}$$

donde r_e, r_P, r_s, $\Sigma_{0,e}$, $\Sigma_{0,P}$ y $\Sigma_{0,s}$ representan los radios de escala y las densidades centrales, mientras que r_c, r_t y k corresponden al radio de núcleo, radio de maréa y una constante arbitraria. El parámetro n indica la medida de concentración (King, 1962; Plummer, 1911; Sersic, 1968).

Galaxia esferoidal enana Sculptor

Galaxia esferoidal enana Sculptor

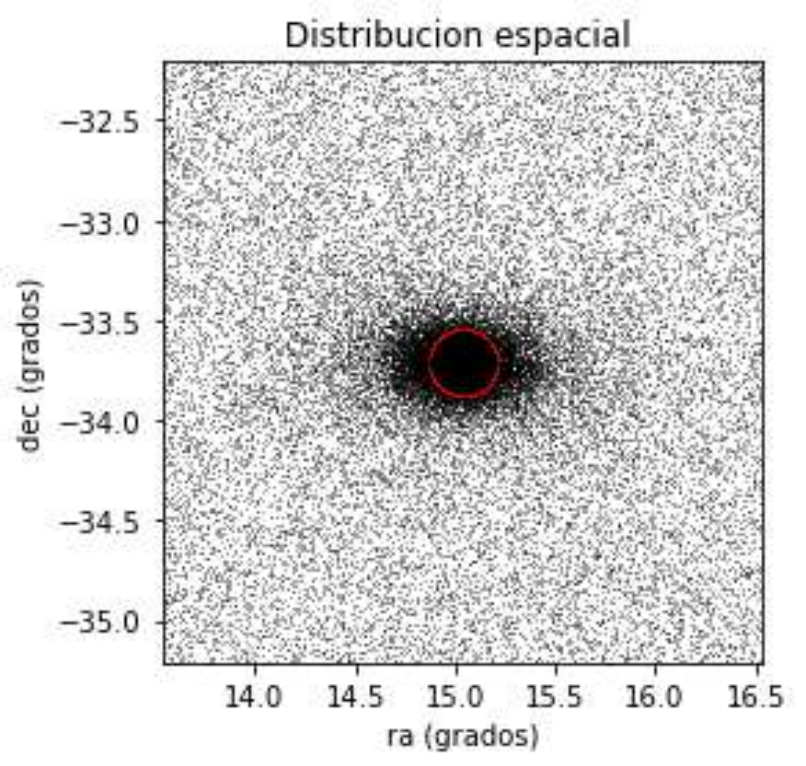

(g) Distribución espacial.

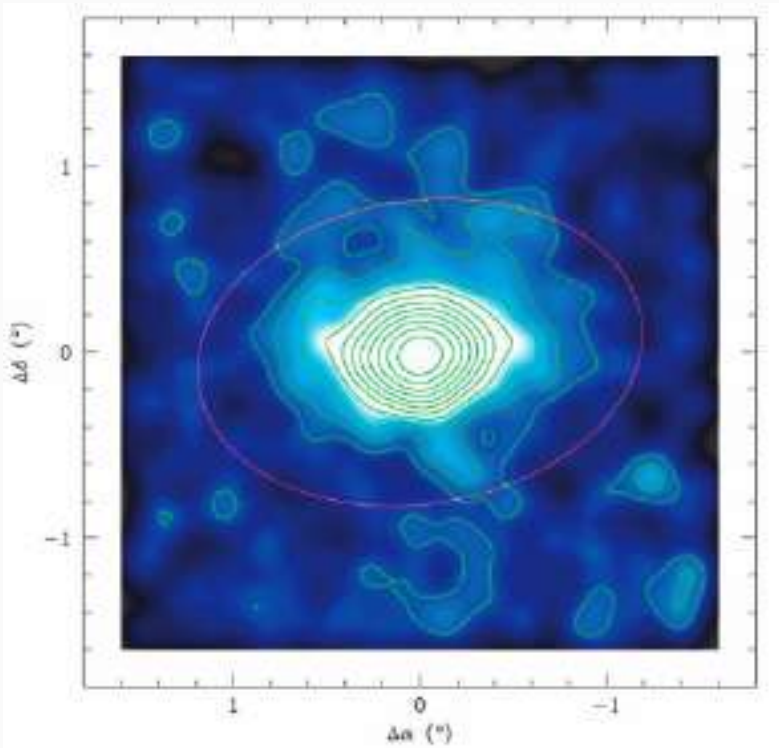

(h) Mapa de contorno (Coleman et al., 2005).

Datos obtenidos del observatorio de Siding Spring.

Galaxia esferoidal enana Sculptor

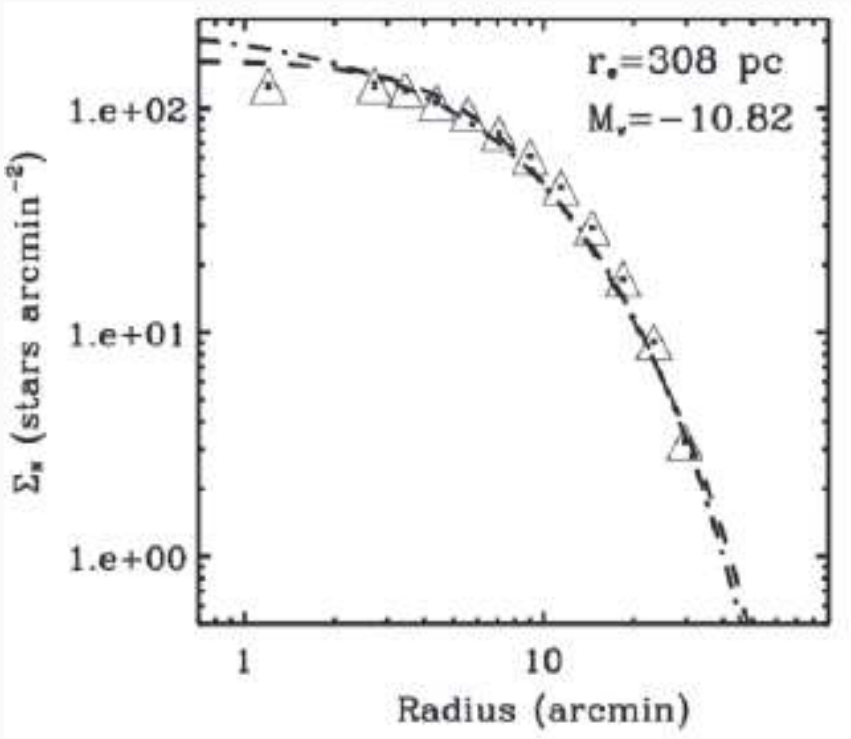

(i) Ajuste del modelo de King y Sersic.

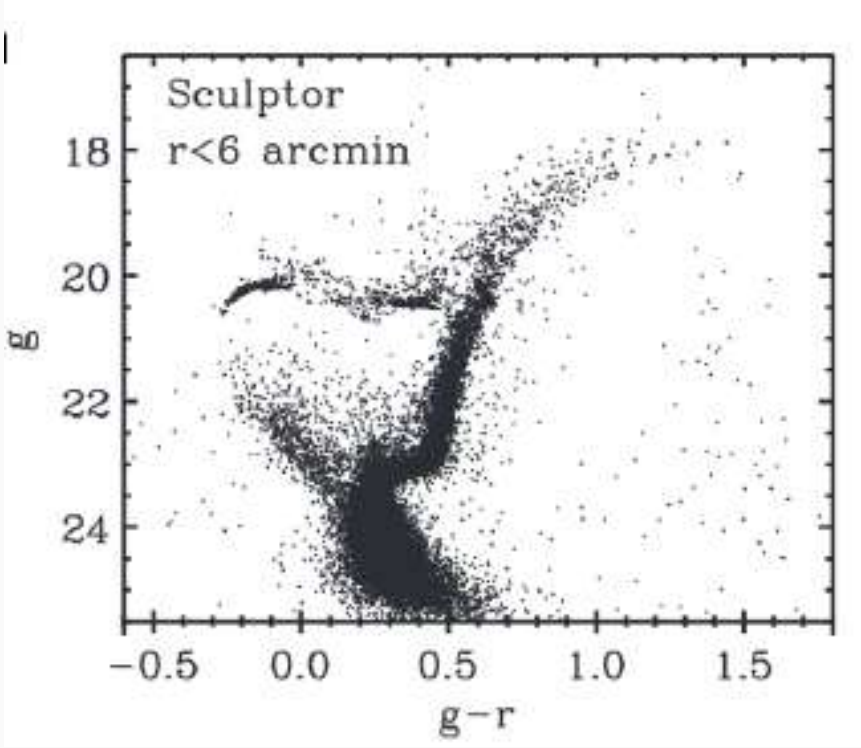

(j) Diagrama color-magnitud (Muñoz et al., 2018).

Datos del telescopio de Magellan-Clay.

¿Realmente no existen picos de sobredensidad estelar en la vecindad de la galaxia esferoidal enana Sculptor?

Proyecto:

SCULPTOR: propiedades físicas y búsqueda por picos de sobredensidad estelar en las afueras de la galaxia esferoidal enana usando los datos del *Dark Energy Survey*

Objetivo General:

El presente trabajo busca determinar los parámetros físicos de Sculptor dSph y realizar una búsqueda de subestructuras en su poblacion estelar..

Datos

Datos de la segunda liberación de los datos del DES, basada en imágenes ópticas e infrarrojas cercanas obtenidas por la DECam (*Dark Energy Camera*; Flaugher et al., 2015) montada en el foco principal del telescopio Blanco de 4 m situado en el Cerro Tololo Interamerican Observatory (CTIO), con un gran campo de cobertura ($\sim 5000\,\mathrm{grados}^2$) del hemisfério sur ecuatorial y excelente calidad.

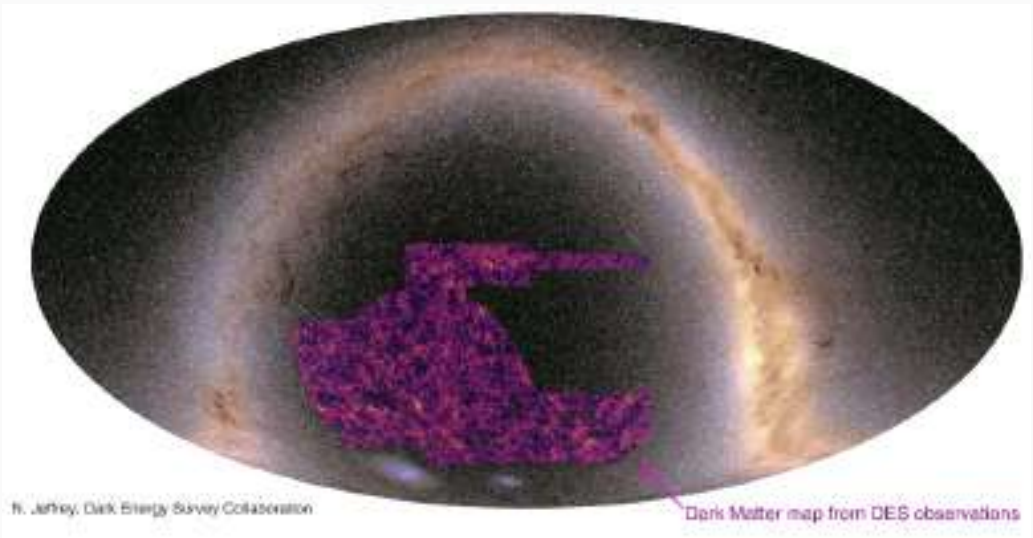

Figure 7: Campo de cobertura del DES [15]

[15] https://des.ncsa.illinois.edu/releases/y3a2

Métodos de análisis

- Un método estadístico basado en la función de verosimilitud

$$\mathcal{L}(\theta_1, \theta_2, \ldots, \theta_n) = \prod_i \ell_i(\theta_1, \theta_2, \ldots, \theta_n)$$

  donde $\ell_i(\theta_1, \theta_2, \ldots, \theta_n)$ es la probabilidad de encontrar el dato observado i dado el conjunto de parámetros $\theta_1, \theta_2, \ldots, \theta_n$.

- Cuatro diferentes modelos de perfiles de densidad radial, King (King, 1962), Plummer (Plummer, 1911), Exponencial y Sersic (Sersic, 1968).

- Ajuste de isócronas para encontrar las propiedades de la población estelar, edad y metalicidad en base a su diagrama color-magnitud (CMD). Aquí, el módulo de distancia es definido como

$$m - M = 5 \log D - 5$$

  donde m, M, D son la magnitud aparente, magnitud absoluta y la distancia del sistema estelar en parsec, respectivamente.

Isócronas de parsec[16]

Modelos de evolución estelar para estrellas con las mismas edad y metalicidad pero con diferentes masas.

[16] http://stev.oapd.inaf.it/cgi-bin/cmd

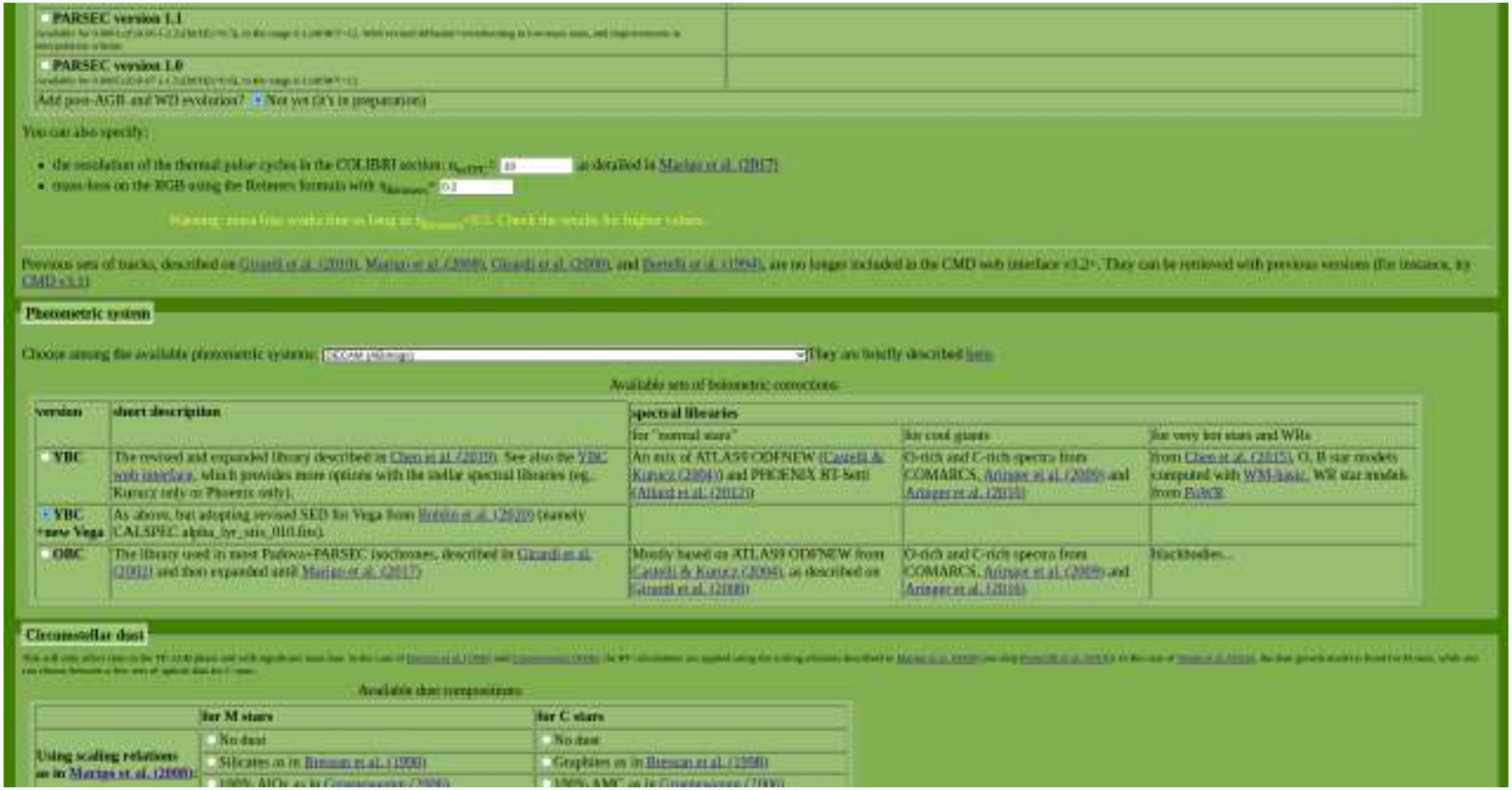

PARSEC version 1.1

PARSEC version 1.0

Add post-AGB and WD evolution? Not yet (it's in preparation)

You can also specify:

- the resolution of the thermal pulse cycles in the COLIBRI section: η_{TPC}= 10 as detailed in Marigo et al. (2017)
- mass-loss on the RGB using the Reimers formula with $\eta_{Reimers}$= 0.2

Warning: mass-loss works fine as long as $\eta_{Reimers}$<0.5. Check the results for higher values.

Previous sets of tracks, described in Girardi et al. (2000), Marigo et al. (2008), Girardi et al. (2008), and Bertelli et al. (1994), are no longer included in the CMD web interface v3.2+. They can be retrieved with previous versions (for instance, try CMD v3.1)

Photometric system

Choose among the available photometric systems: [UCAM (All mags)] They are briefly described here.

Available sets of bolometric corrections

version	short description	spectral libraries		
		for "normal stars"	for cool giants	for very hot stars and WRs
YBC	The revised and expanded library described in Chen et al. (2019). See also the YBC web interface, which provides more options with the stellar spectral libraries (eg., Kurucz only or Phoenix only).	An mix of ATLAS9 ODFNEW (Castelli & Kurucz (2004)) and PHOENIX BT-Settl (Allard et al. (2012))	O-rich and C-rich spectra from COMARCS, Aringer et al. (2009) and Aringer et al. (2016)	from Chen et al. (2015): O, B star models computed with WM-basic. WR star models from PoWR
YBC +new Vega	As above, but adopting revised SED for Vega from Bohlin et al. (2020) (namely CALSPEC alpha_lyr_stis_010.fits).			
OBC	The library used in most Padova+PARSEC isochrones, described in Girardi et al. (2002) and then expanded until Marigo et al. (2017)	Mostly based on ATLAS9 ODFNEW from Castelli & Kurucz (2004), as described in Girardi et al. (2008)	O-rich and C-rich spectra from COMARCS, Aringer et al. (2009) and Aringer et al. (2016)	blackbodies...

Circumstellar dust

Available dust compositions

	for M stars	for C stars
Using scaling relations as in Marigo et al. (2008):	No dust	No dust
	Silicates as in Bressan et al. (1998)	Graphites as in Bressan et al. (1998)
	100% AlOx as in Groenewegen (2006)	100% AMC as in Groenewegen (2006)


as in Marigo et al. (2008):
Silicates as in Bressan et al. (1998)
Graphites as in Bressan et al. (1998)
100% AlOx as in Groenewegen (2006)
100% AMC as in Groenewegen (2006)
60% Silicate + 40% AlOx as in Groenewegen (2006)
85% AMC + 15% SiC as in Groenewegen (2006)
100% Silicate as in Groenewegen (2006)
Other options for C-star dust were discarded starting from CMD v3.7.
Interstellar extinction
Total extinction A_V = 0.0 mag
Apply this extinction
Using extinction coefficients computed star-by-star (except for the OBC case, which uses constant coefficients)
Adopted extinction curve
Cardelli et al. (1989) + O'Donnell (1994), with R_V=3.1
Warning: Interstellar extinction works only for isochrone tables, not for LFs or simulated populations. Moreover, it does not work (yet) on the PARSEC evolution models.
Long Period Variability
We provide three options to simulate long-period variability during the RGB and AGB phase. All three provide the periods for a set of pulsation modes as well as the quantity pmode, whose integer value indicates the radial order of the dominant pulsation mode: 0 is the fundamental mode (FM), 1 the first overtone mode (1OM), and so on. The value -1 indicates that no mode is expected to be excited, or that the stellar parameters are outside the range of validity for computing variability properties.
Prescription
Description
1. Periods from Trabucchi et al. (2017)
FM and 1OM periods from preliminary best-fit relations. These are provided for backwards compatibility and are superseded by the option 2 below.
2. Periods from Trabucchi et al. (2019)
Periods for the FM, 1OM, 2OM, 3OM, and 4OM. They are derived from best-fit relations based on linear pulsation models, so this is the most appropriate option for who is interested in studying overtone mode pulsation, but is not appropriate for the FM. Note: as an alternative, you can use Trabucchi's pulsation code, which will include the growth rates.
3. Periods from Trabucchi et al. (2021)
Same as the option 2 except that the FM period and the regime in which it is dominant (i.e. when pmode=0) are determined from non-linear pulsation models. This option is the most appropriate for studying the FM.
Cautionary remarks When options 2 or 3 are used, most stars with small luminosity/mass ratio are assigned a value pmode=4. This does not necessarily mean that the 4th overtone is really dominant. Indeed, there seems to be no clear observational detection of the 4th overtone mode in AGB stars, suggesting that it either is stable or has very small amplitude (see Trabucchi et al. (2017)). Therefore it is reasonable to interpret the occurrences of pmode=4 as an indication that the star displays only small-amplitude oscillations, if any. The origin of this patter is the following. The prescription from Trabucchi et al. (2019) used to assign the value of pmode exploits the fact that the dominant mode shifts towards pulsation modes of increasingly smaller radial order as the stellar luminosity increase. This is achieved by comparing the actual luminosity of a simulated star with the value of luminosity corresponding to the transition between two pulsation modes. Since the pulsation models of Trabucchi et al. (2019) do not include properties of pulsation modes higher than the 4th overtone, there is no prediction for the lower luminosity boundary of the regime in which it is dominant.
Initial mass function
The IMF will be used to compute the stellar occupation along the isochrones, and to compute integrated magnitudes, LFs, etc. (see section Output below)
IMF for single stars:
Ages/metallicities

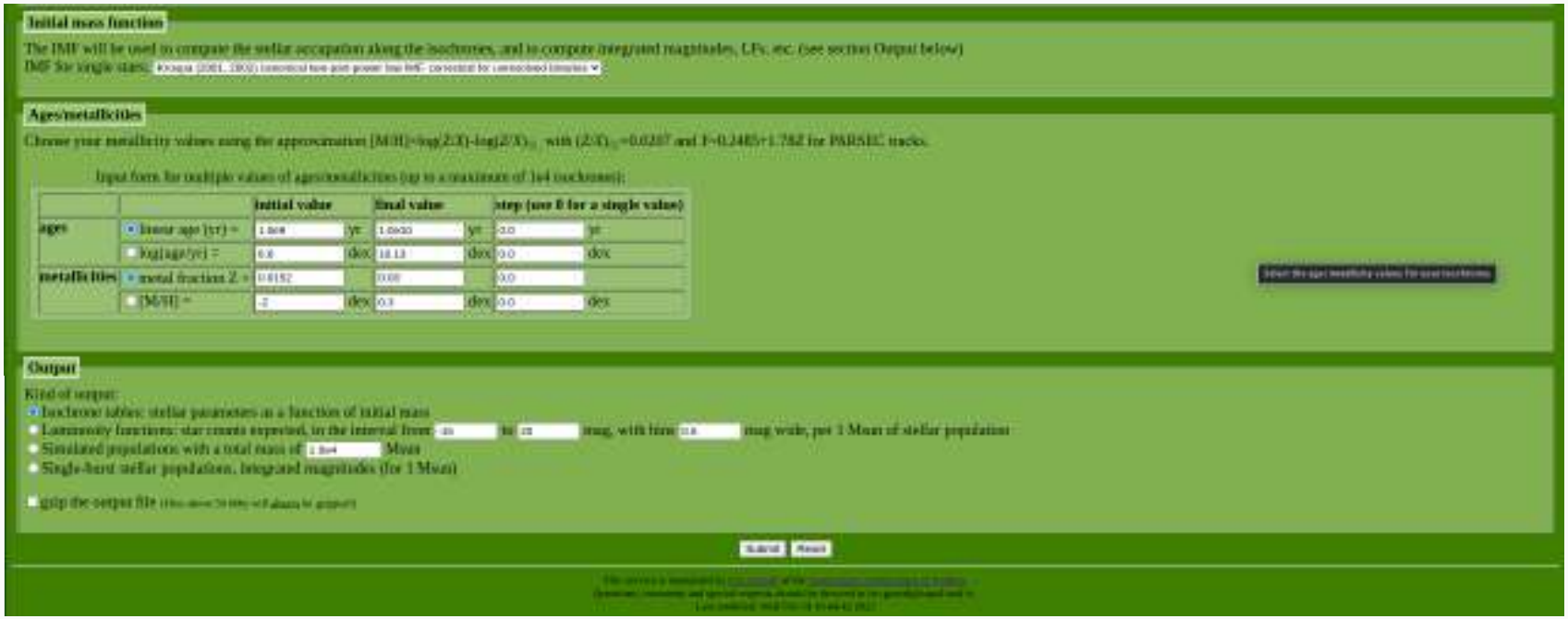
Initial mass function
The IMF will be used to compute the stellar occupation along the isochrones, and to compute integrated magnitudes, LFs, etc. (see section Output below)
IMF for single stars:
Ages/metallicities
Choose your metallicity values using the approximation [M/H]=log(Z/X)-log(Z/X)⊙ with (Z/X)⊙=0.0207 and Y=0.2485+1.78Z for PARSEC tracks.
Input form for multiple values of ages/metallicities (up to a maximum of 364 isochrones):
initial value
final value
step (use 0 for a single value)
ages
Linear age [yr] =
1.0e8
yr
1.0e10
yr
0.0
yr
log(age/yr) =
8.0
dex
10.13
dex
0.0
dex
metallicities
metal fraction Z =
0.0152
0.00
0.0
[M/H] =
-2
dex
0.3
dex
0.0
dex
Output
Kind of output:
Isochrone tables: stellar parameters as a function of initial mass
Luminosity functions: star counts expected, in the interval from
to
mag, with bins
mag wide, per 1 Msun of stellar population
Simulated populations with a total mass of
1.0e4
Msun
Single-burst stellar population, integrated magnitudes (for 1 Msun)
gzip the output file
Submit
Reset

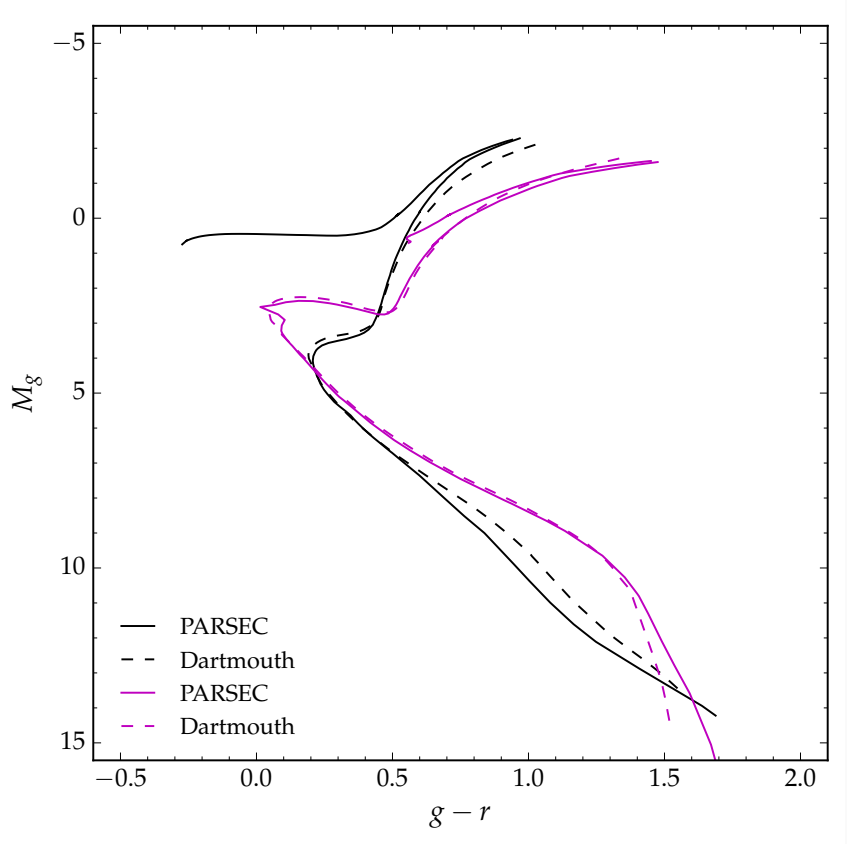

Figure 8: Figura extraída de Luque Canaza (2018). Modelos de isócronas de PARSEC y Dartmouth. La línea sólida (discontinua) de color magenta representa un modelo de isócrona de PARSEC (Dartmouth) con edad 3 G años y metalicidad $Z = 0.003$, mientras que la línea sólida (discontinua) negra representa un modelo de isócrona de PARSEC (Dartmouth) con edad 13.3 G años y Z = 0.00012. Para las isócronas de Dartmouth fueron usados, respectivamente, $[Fe/H] = 0.75(Z = 0.003)$ y $[Fe/H] = 2.23(Z = 0.00012)$, para el modelo de edad intermedia y vieja. Los modelos de PARSEC incluyen la región de la quema de helio en el núcleo, mientras que los modelos de Dartmouth no incluyen.

- Para la búsqueda de posibles sobredensidades estelares en la vecindad de esta galaxia se usará el código SPARSEX (Luque et al., 2016).

Salida de SPARSEX

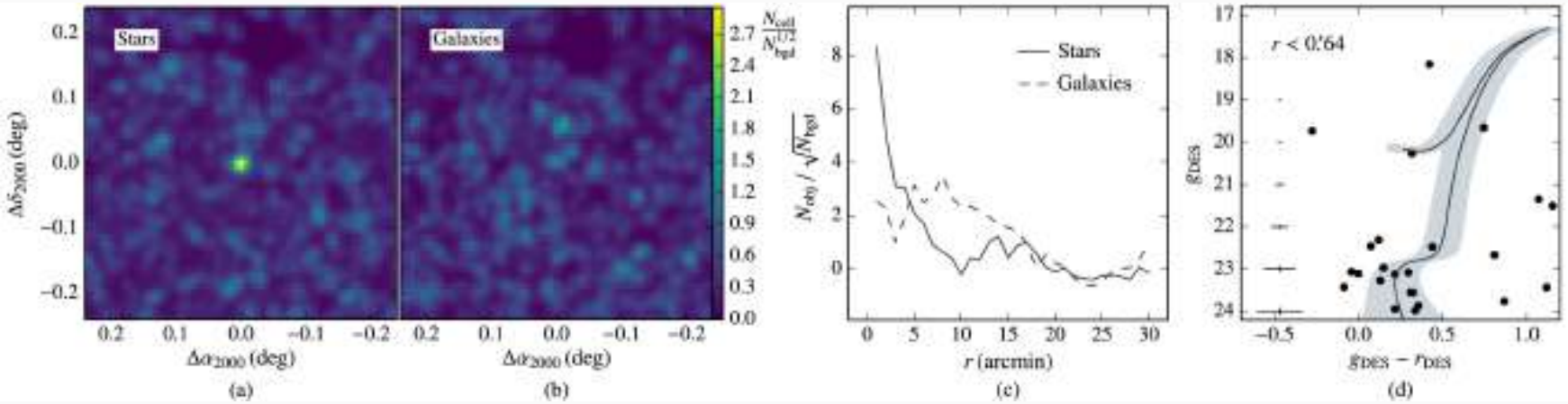

Figure 9: a) y b) Mapas de densidad. c) Perfil de significancia. d) CMD y modelo de PARSEC, para el cúmulo estelar DES 3 (Luque et al., 2018).

Técnicas de análisis: Implementación computacional

Representación espacial y CMD de Sculptor usando los datos del DES.

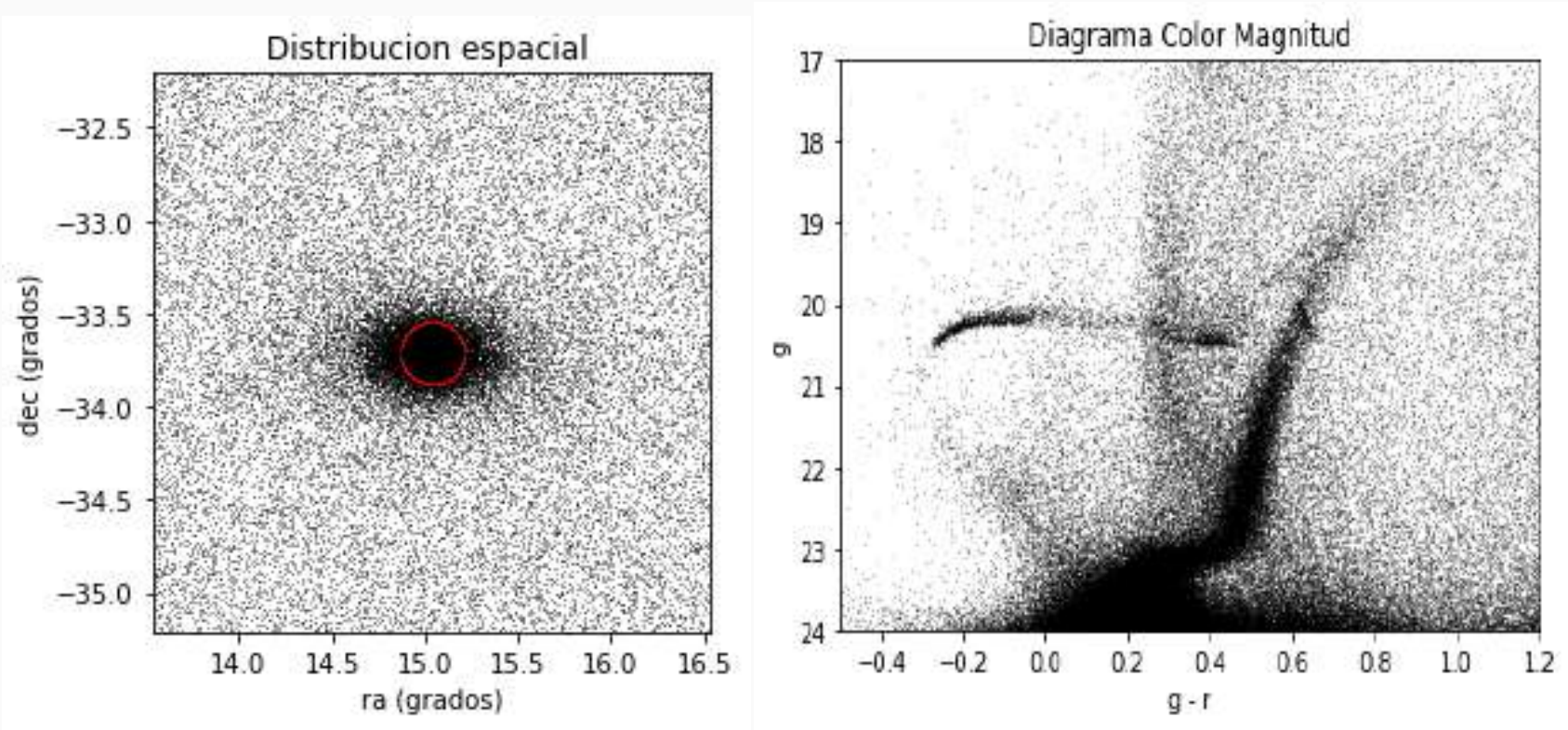

Figure 10: Panel de la izquierda: distribución espacial de fuentes clasificadas como estrellas alrededor de Sculptor. Un círculo (color rojo) de 10 arcmin de radio centrado en Sculptor es también mostrado. Panel de la derecha. CMD de Sculptor construido con estrellas contenidas dentro del círculo mostrado en el panel de la izquierda.

Ajuste de modelos de perfil de densidad

Modelo exponencial

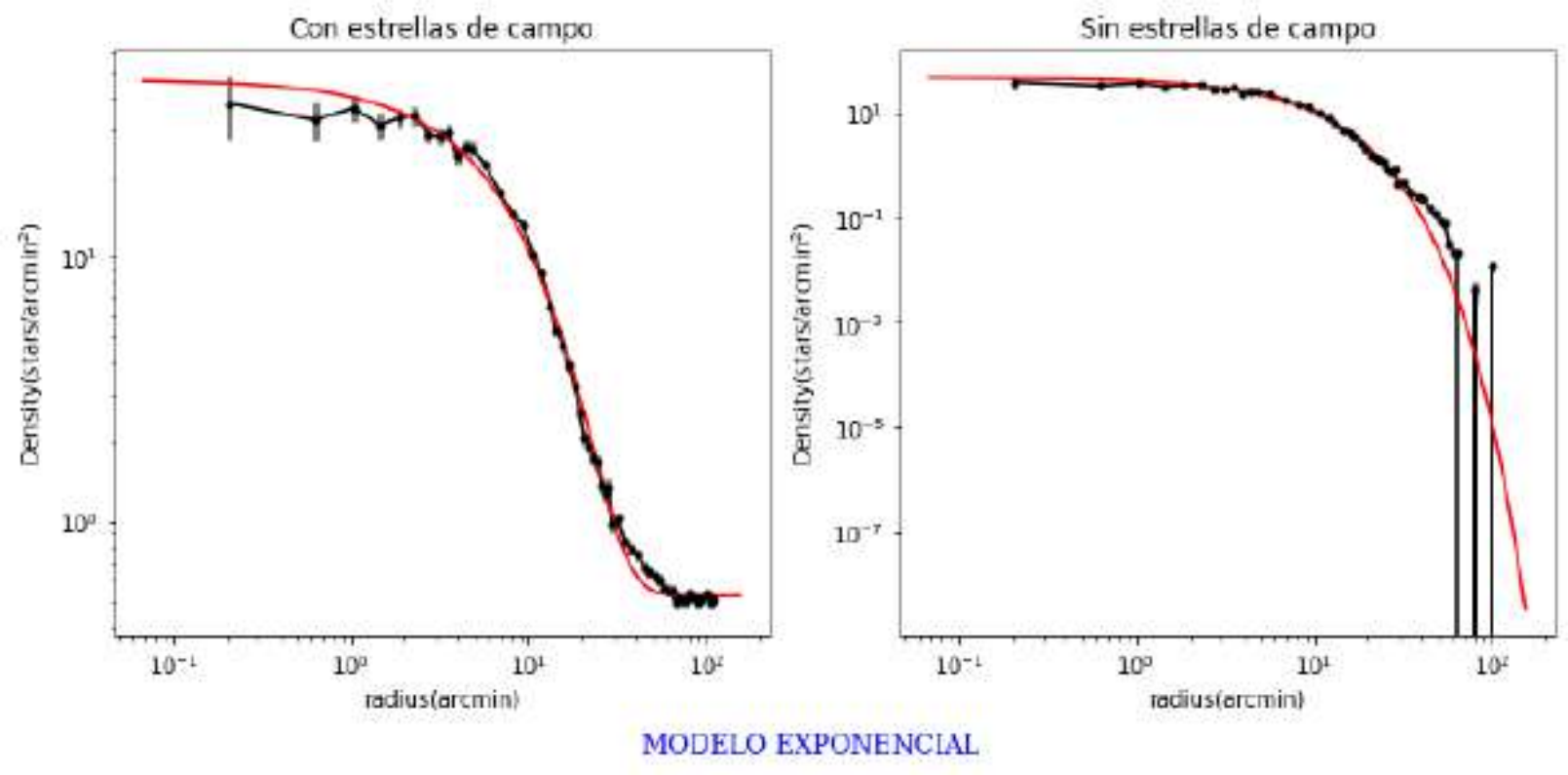

Figure 11: Panel de la izquierda: los círculos sólidos respresentan el perfil de densidad observado, mientras que la línea sólida roja es la combinación del mejor ajuste del modelo exponencial y la densidad de campo. Panel de la derecha: los círculos sólidos respresentan el perfil de densidad de Sculptor, mientras que la línea sólida roja es el mejor ajuste del modelo exponencial. En ambos paneles, las barras de errores representan 1σ de las incertidumbres de Poisson.

Probabilidades Marginalizadas para los parámetros del modelo exponencial

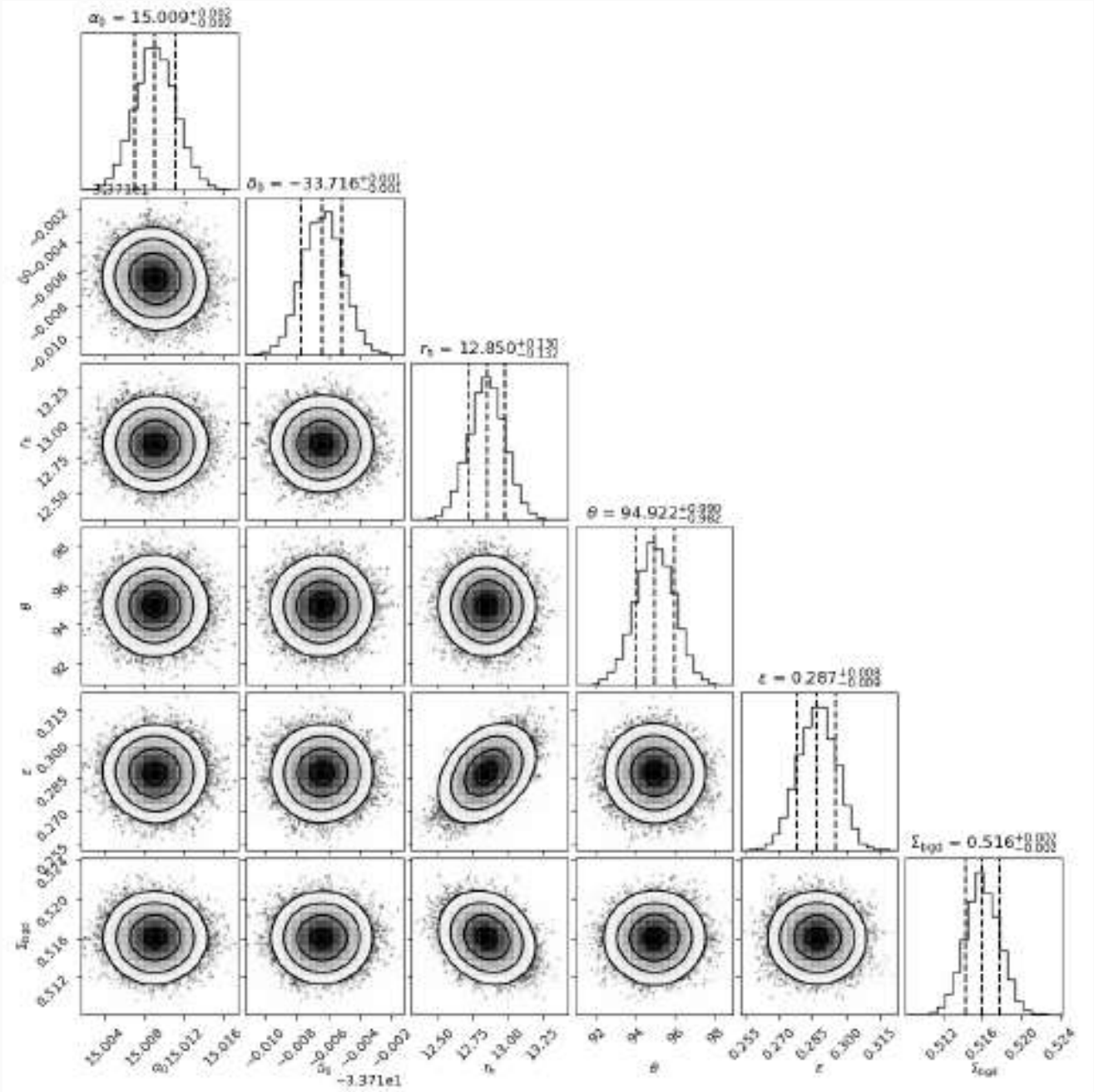

Modelo de Plummer

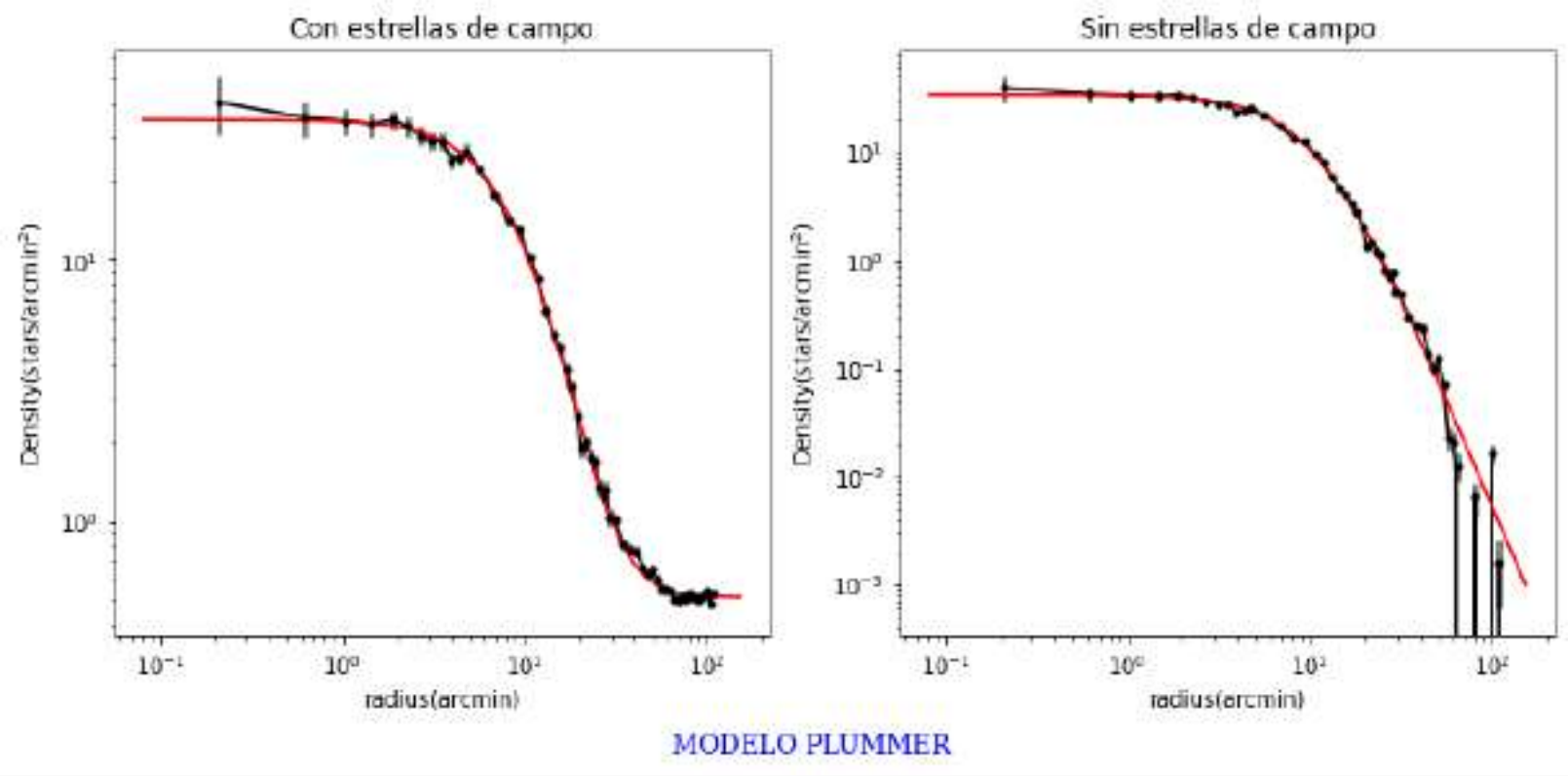

Figure 12: Panel de la izquierda: los círculos sólidos respresentan el perfil de densidad observado, mientras que la línea sólida roja es la combinación del mejor ajuste del modelo de Plummer y la densidad de campo. Panel de la derecha: los círculos sólidos respresentan el perfil de densidad de Sculptor, mientras que la línea sólida roja es el mejor ajuste del modelo de Plummer. En ambos paneles, las barras de errores representan 1σ de las incertidumbres de Poisson.

Probabilidades Marginalizadas para los parámetros del modelo de Plummer

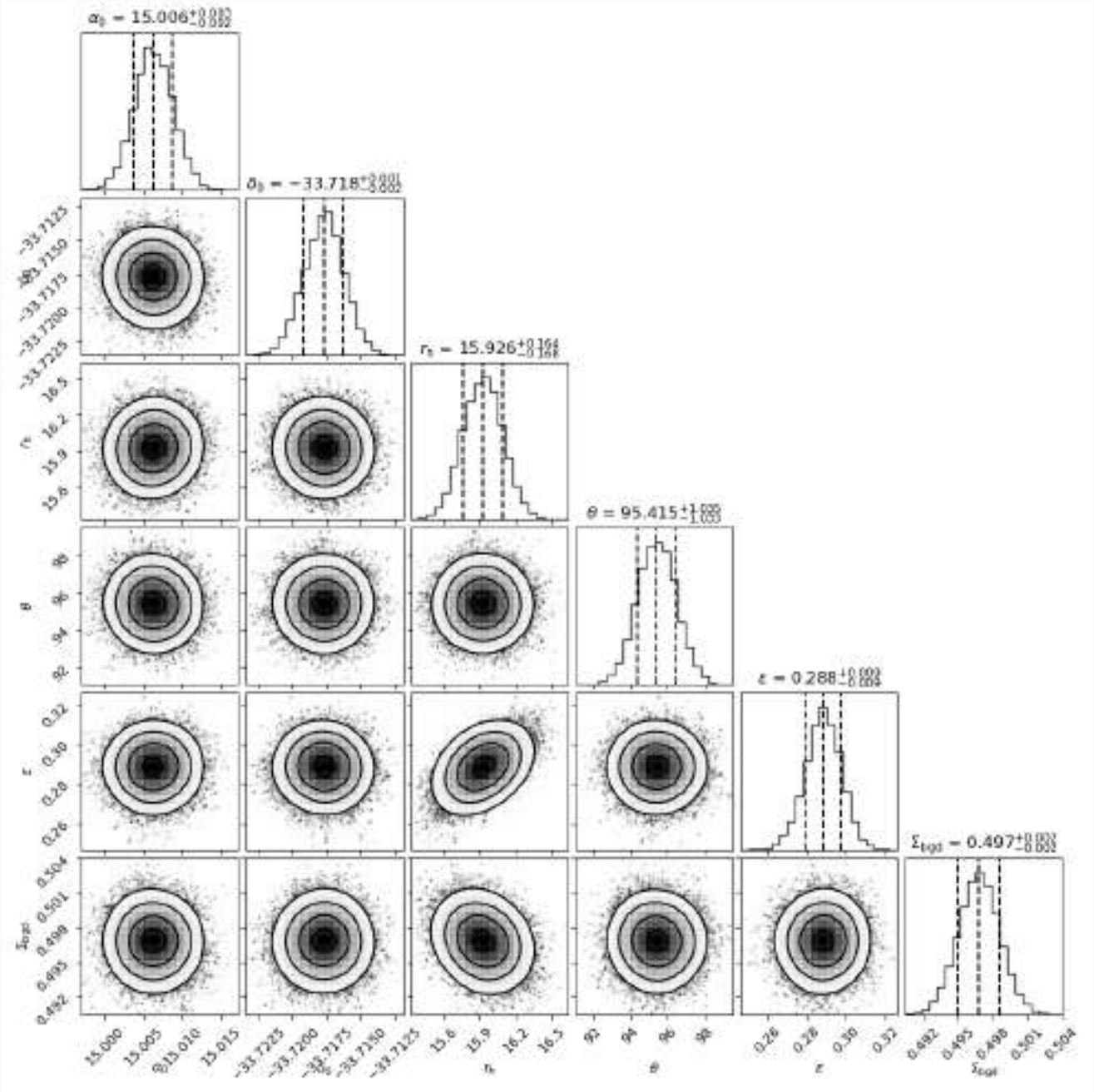

Modelo de King

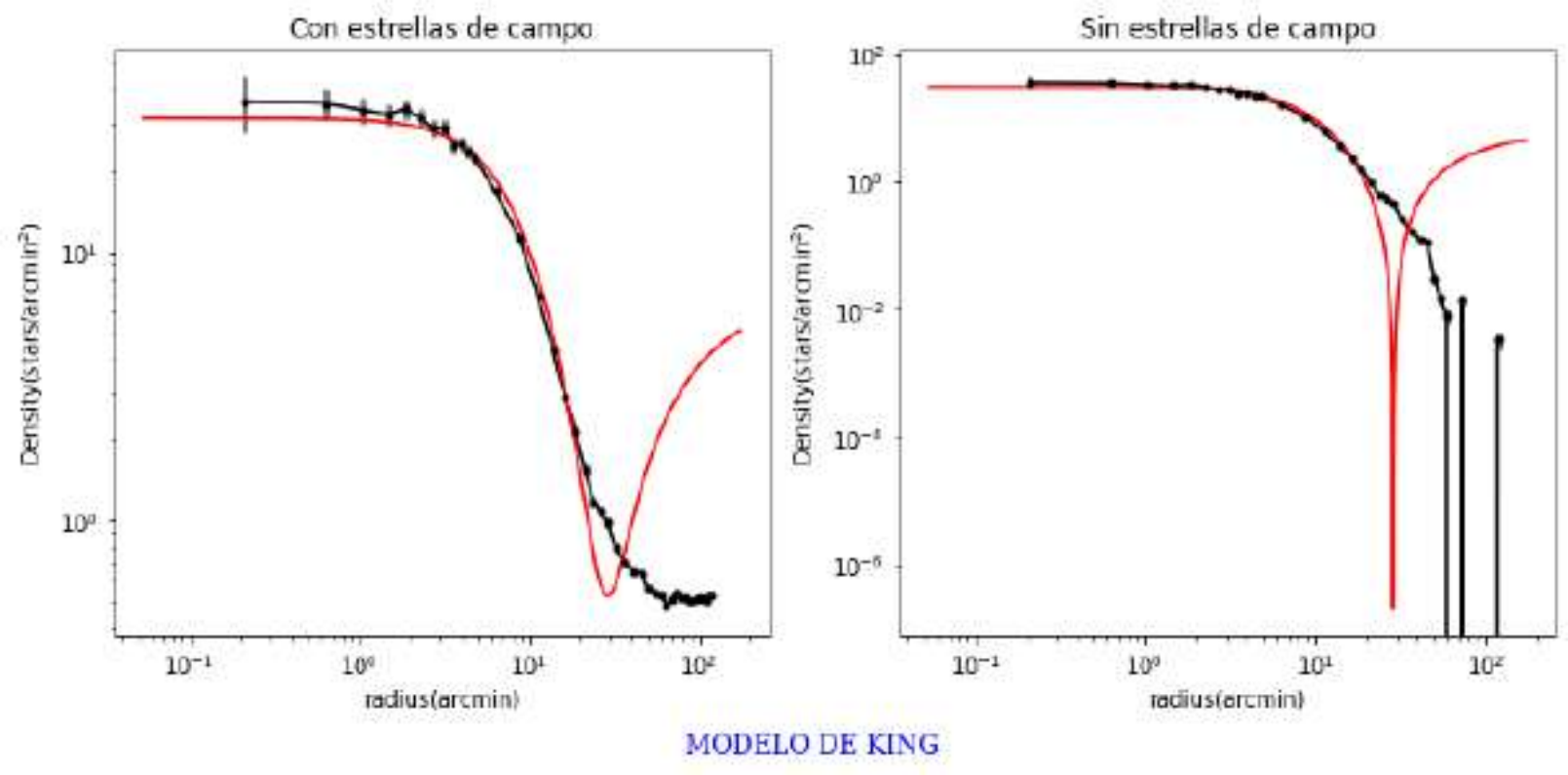

Figure 14: Panel de la izquierda: los círculos sólidos respresentan el perfil de densidad observado, mientras que la línea sólida roja es la combinación del mejor ajuste del modelo de King y la densidad de campo. Panel de la derecha: los círculos sólidos respresentan el perfil de densidad de Sculptor, mientras que la línea sólida roja es el mejor ajuste del modelo de King. En ambos paneles, las barras de errores representan 1σ de las incertidumbres de Poisson.

Probabilidades Marginalizadas para los parámetros del modelo de King

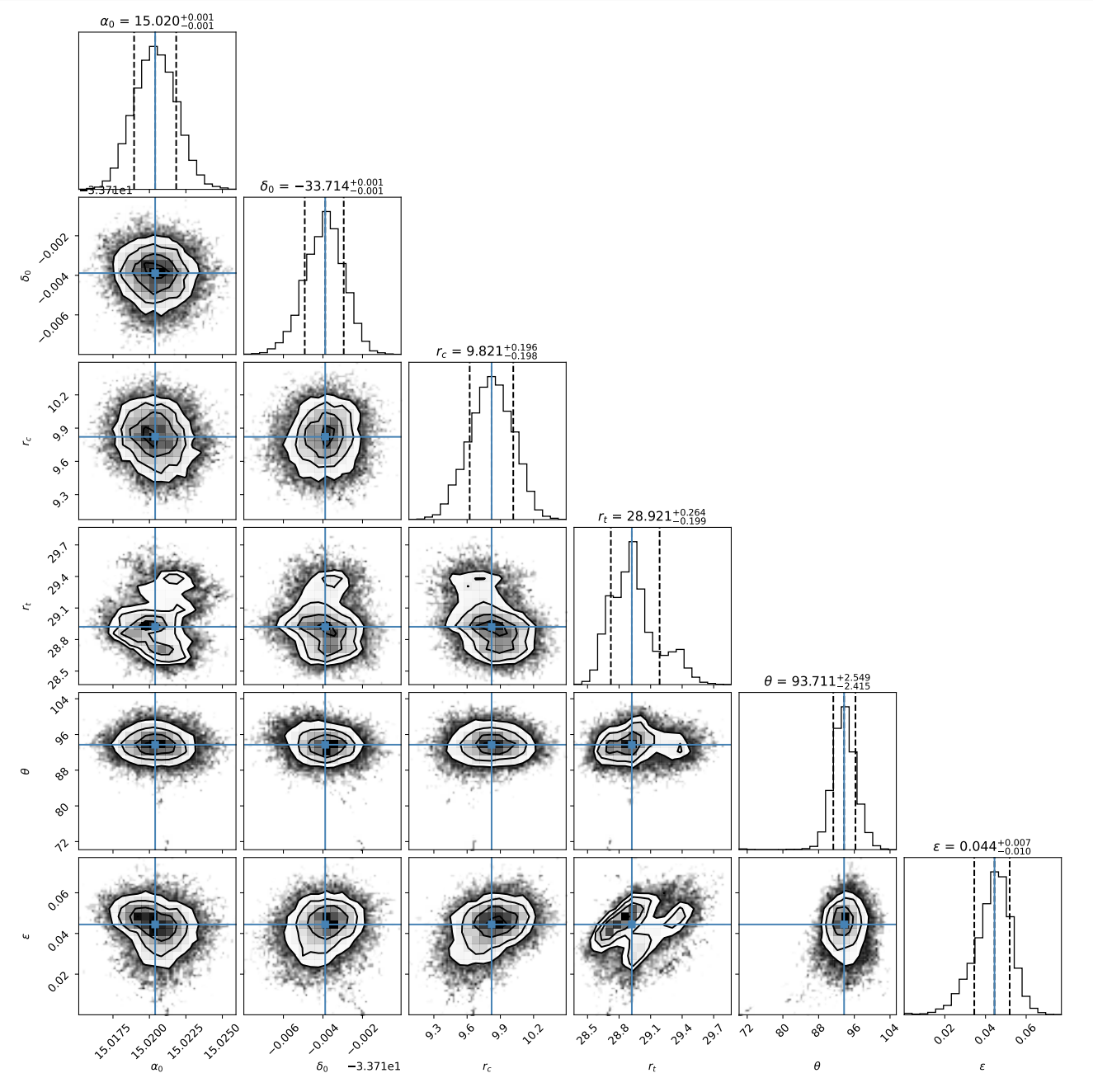

Modelo de Sersic

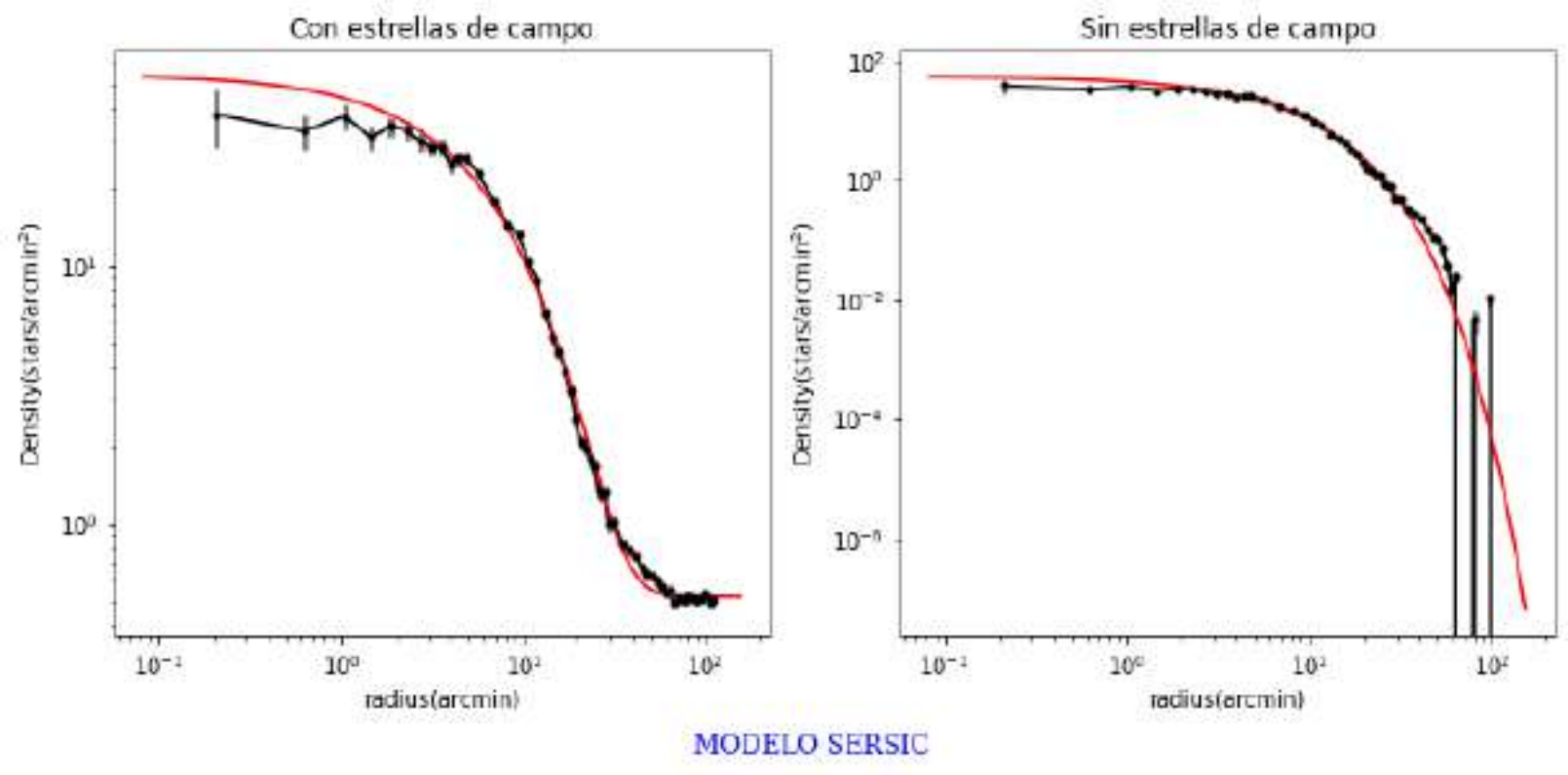

Figure 15: Panel de la izquierda: los círculos sólidos respresentan el perfil de densidad observado, mientras que la línea sólida roja es la combinación del mejor ajuste del modelo de Sersic y la densidad de campo. Panel de la derecha: los círculos sólidos respresentan el perfil de densidad de Sculptor, mientras que la línea sólida roja es el mejor ajuste del modelo de Sersic. En ambos paneles, las barras de errores representan 1σ de las incertidumbres de Poisson.

Probabilidades Marginalizadas para los parámetros del modelo de Sersic

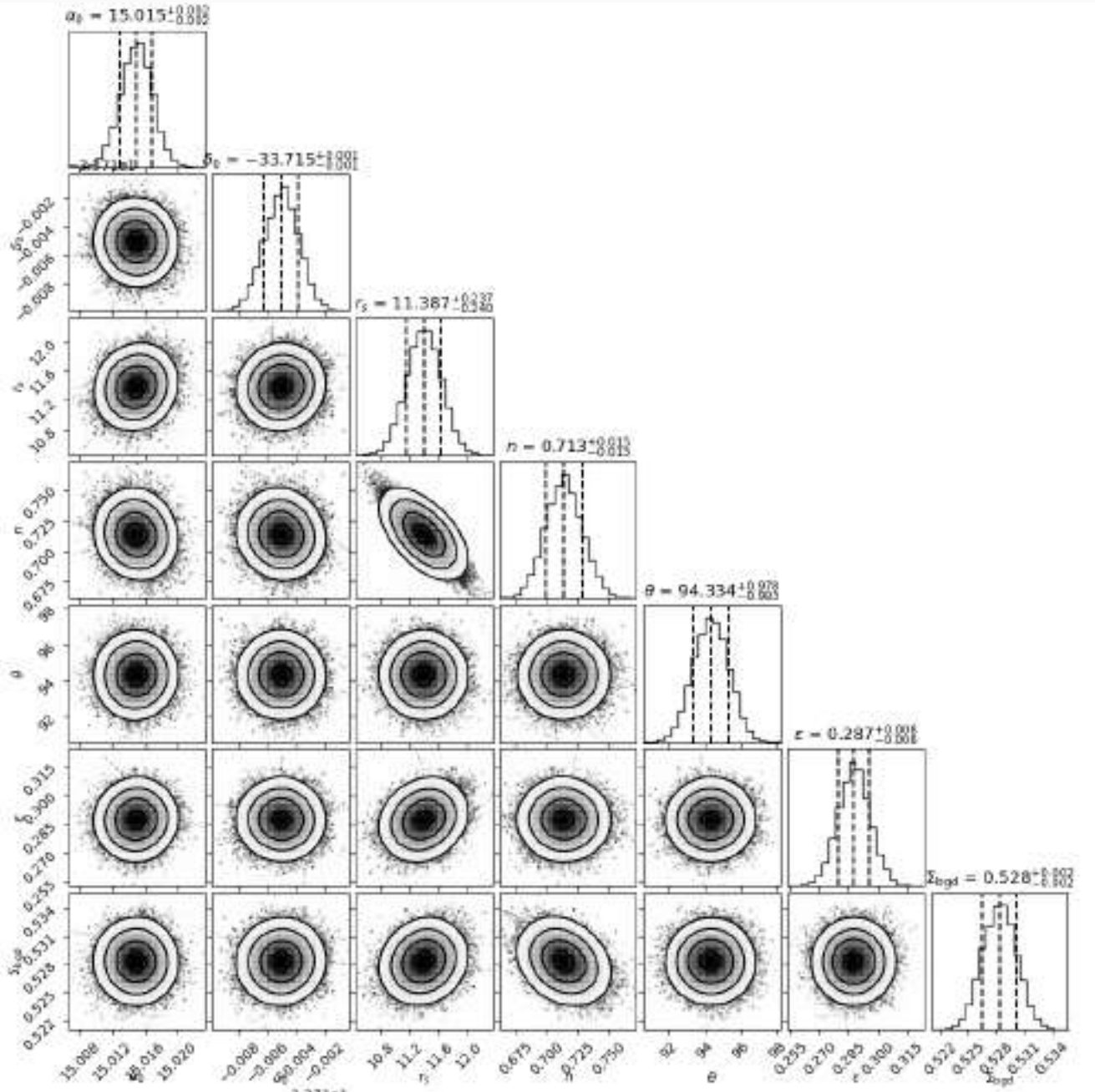

¿Problema en la región central de Sculptor?

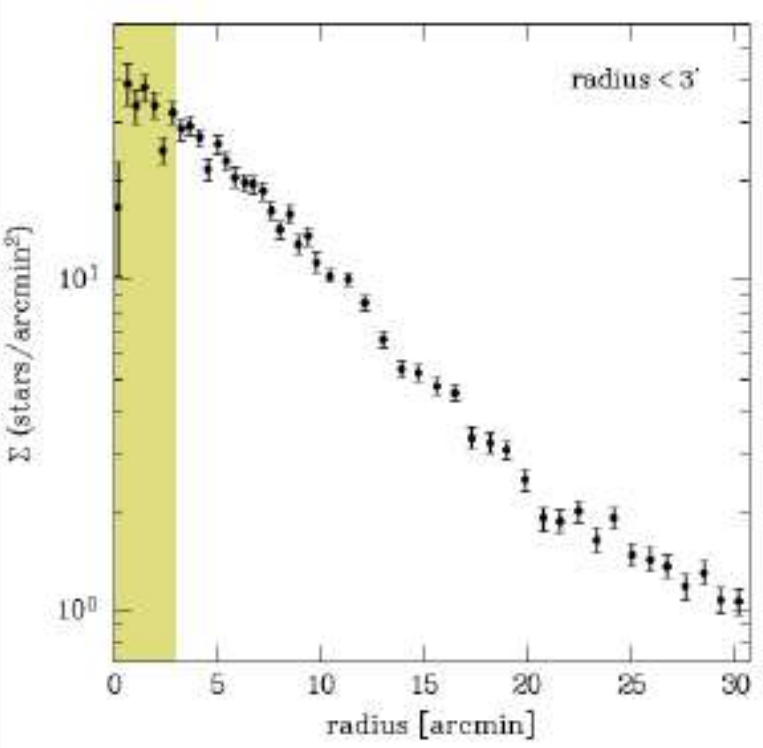

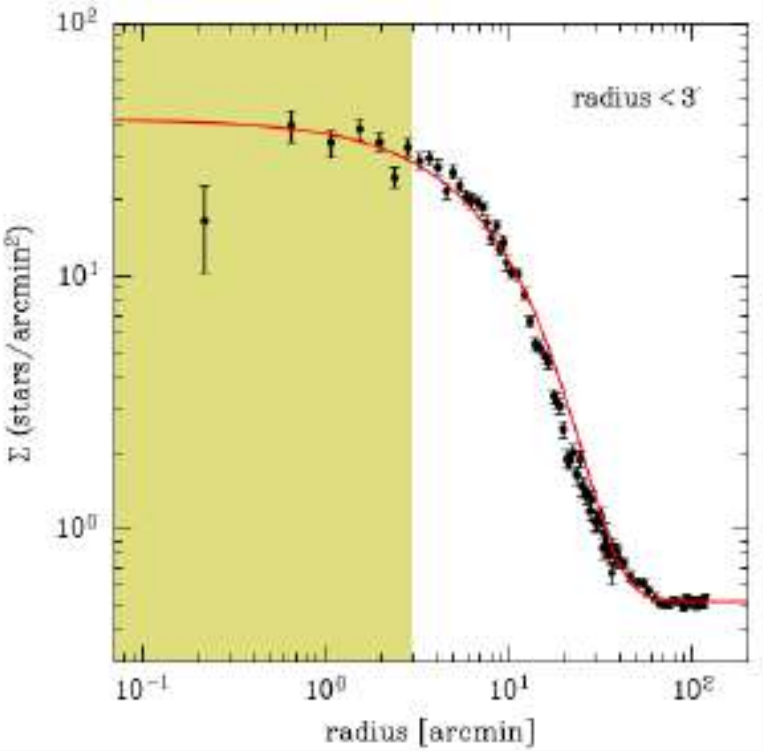

Mapas de sobredensidad

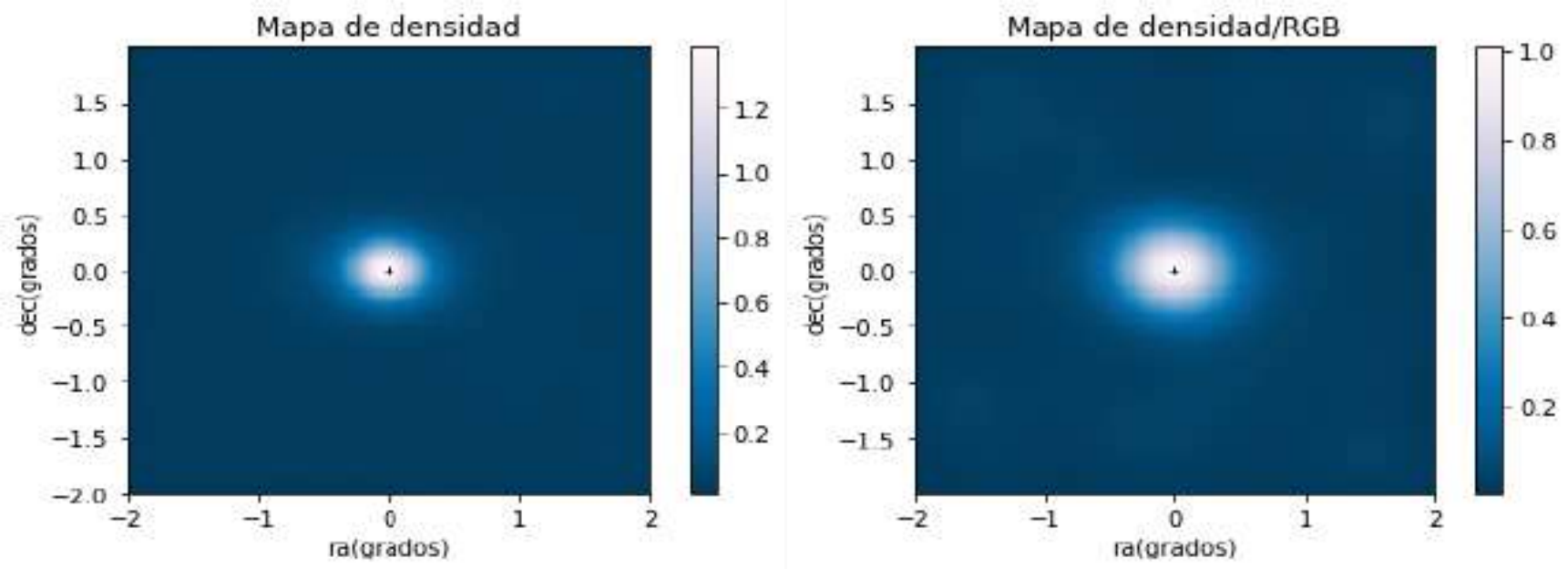

Figure 16: Panel de la izquierda: mapa de densidad para todas las estrellas de Sculptor. Panel de la izquierda: mapa de densidad contruído solo con estrellas de la RGB.

No se encontraron sobredensidades usando mapas de densidad.

¡Es la hora del algoritmo SparSeX!

¿Cómo ajustar una isócrona?

De la definición de magnitud aparente m tenemos

$$m = -2.5 \log(F) \tag{5}$$

donde F es el flujo del sistema.
De la ecuación (1) se deriva las siguientes ecuaciones

$$g = M_g + (m - M)_0 + Ag$$
$$r = M_r + (m - M)_0 + Ar$$

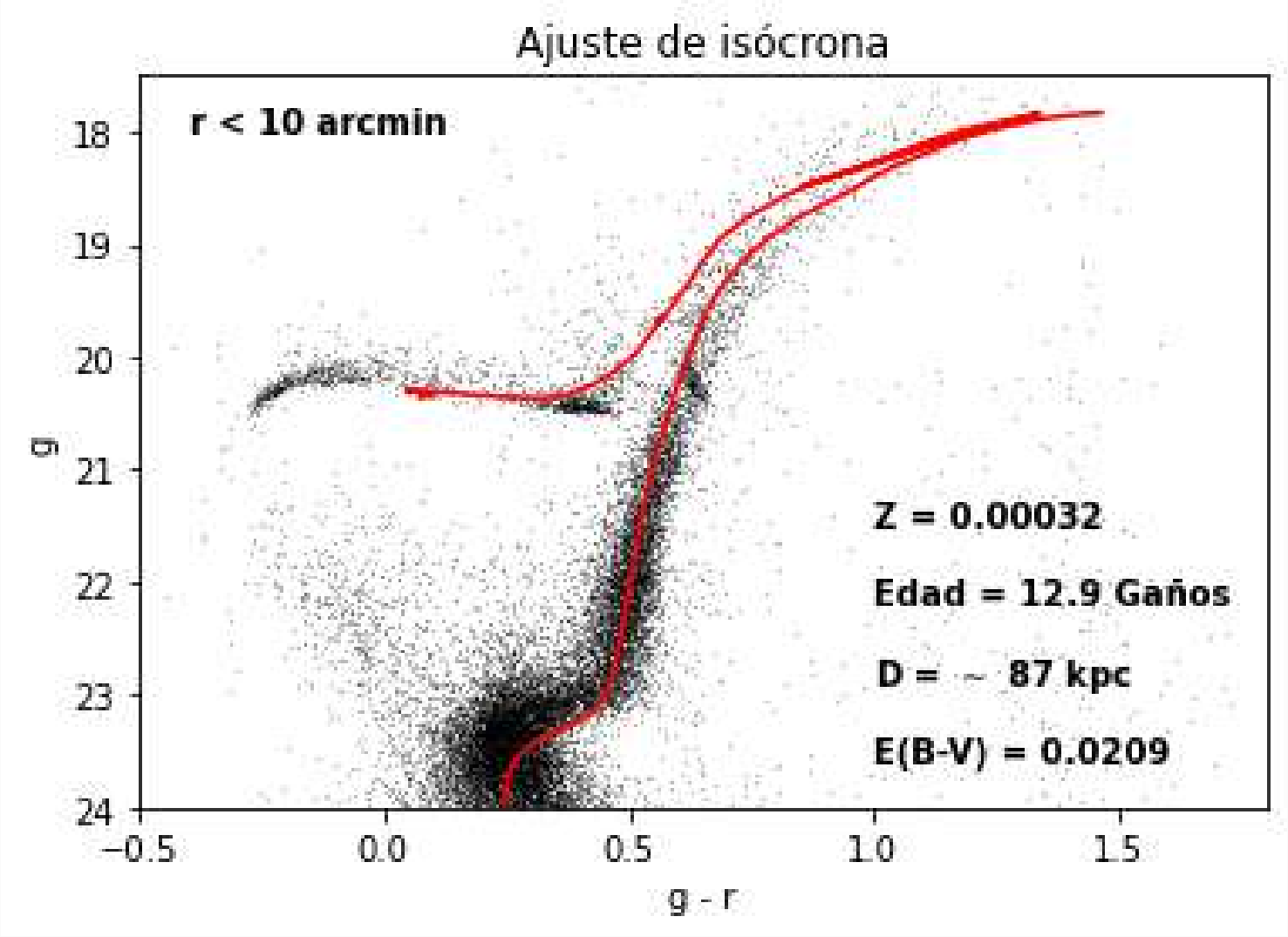

Figure 17: CMD de Sculptor construído usando estrellas dentro de un radio de 10 arcmin centrado en Sculptor. Los parámetros del modelo de isócrona de Parsec (línea roja) son presentados en el panel.

Gracias por su atención

Referencias

References

Coleman, M. G., Da Costa, G. S., & Bland-Hawthorn, J. (2005, September). The Absence of Extratidal Structure in the Sculptor Dwarf Spheroidal Galaxy. , *130*(3), 1065-1082. doi: 10.1086/432662

Flaugher, B., Diehl, H. T., Honscheid, K., Abbott, T. M. C., Alvarez, O., Angstadt, R., ... DES Collaboration (2015, November). The Dark Energy Camera. , *150*(5), 150. doi: 10.1088/0004-6256/150/5/150

Hodge, P. W. (1961, October). The distribution of stars in the Sculptor dwarf galaxy. , *66*, 384. doi: 10.1086/108443

King, I. (1962, October). The structure of star clusters. I. an empirical density law. , *67*, 471. doi: 10.1086/108756

Referencias ii

Luque, E., Queiroz, A., Santiago, B., Pieres, A., Balbinot, E., Bechtol, K., ... Zhang, Y. (2016, May). Digging deeper into the Southern skies: a compact Milky Way companion discovered in first-year Dark Energy Survey data. , *458*(1), 603-612. doi: 10.1093/mnras/stw302

Luque, E., Santiago, B., Pieres, A., Marshall, J. L., Pace, A. B., Kron, R., ... Thomas, D. (2018, August). Deep SOAR follow-up photometry of two Milky Way outer-halo companions discovered with Dark Energy Survey. , *478*(2), 2006-2018. doi: 10.1093/mnras/sty1039

Luque Canaza, E. F. (2018). Determinación de las propiedades físicas de diez compañeros de la vía láctea descubiertos en los datos del primer año de observación del dark energy survey.

Referencias iii

Muñoz, R. R., Côté, P., Santana, F. A., Geha, M., Simon, J. D., Oyarzún, G. A., … Djorgovski, S. G. (2018, June). A MegaCam Survey of Outer Halo Satellites. III. Photometric and Structural Parameters. , *860*(1), 66. doi: 10.3847/1538-4357/aac16b

Plummer, H. C. (1911, March). On the problem of distribution in globular star clusters. , *71*, 460-470. doi: 10.1093/mnras/71.5.460

Sersic, J. L. (1968). *Atlas de Galaxias Australes*.

Wang, M. Y., de Boer, T., Pieres, A., Li, T. S., Drlica-Wagner, A., Koposov, S. E., … DES Collaboration (2019, August). The Morphology and Structure of Stellar Populations in the Fornax Dwarf Spheroidal Galaxy from Dark Energy Survey Data. , *881*(2), 118. doi: 10.3847/1538-4357/ab31a9